Title

Local Synthesis of Reticulon-1C Lessens the Outgrowth of Injured Axons by Controlling Spastin Activity

Authors

Alejandro Luarte[1,2,3]*, Javiera Gallardo[8], Daniela Corvalán[1,2], Ankush Chakraborty [1,2], Cláudio Gouveia-Roque[5], Francisca Bertin[11], Carlos Contreras[1,2], Juan Pablo Ramírez [1,2], Andrè Weber[20], Waldo Acevedo[8], Werner Zuschratter[19], Rodrigo Herrera-Molina[9,10], Úrsula Wyneken [1,2,3] Andrea Paula-Lima [16,17], Tatiana Adasme-Rocha[18], Antonia Figueroa[1,2], Carolina González[15], Christian González-Billault[4, 12, 13, 14], Ulrich Hengst [5,6], and Andrés Couve [4]

Affiliations

1 Faculty of Medicine, Universidad de los Andes, Santiago 7620001, Chile
2 Program in Neuroscience, Center for Biomedical Research, and Innovation (CiiB), Universidad de los Andes, Santiago 7620001, Chile
3 IMPACT, Center of Interventional Medicine for Precision and Advanced Cellular Therapy, Santiago 7620001, Chile
4 Department of Neuroscience, Faculty of Medicine, Universidad de Chile, Santiago, Chile.
5 The Taub Institute for Research on Alzheimer's Disease and the Aging Brain, Columbia University Vagelos College of Physicians and Surgeons, New York, NY 10032, USA
6 Department of Pathology and Cell Biology, Columbia University Vagelos College of Physicians and Surgeons, New York, NY 10032, USA
7 Instituto de Química, Facultad de Ciencias, Pontificia Universidad Católica de Valparaíso, Valparaíso 2373223, Chile
8 Centro de Medicina Regenerativa, Facultad de Medicina, Clínica Alemana-Universidad del Desarrollo, Santiago, Chile
9 Centro Integrativo de Biología y Química Aplicada, Universidad Bernardo O'Higgins, 8307993 Santiago, Chile
10 Department of Pharmacology & Physiology, George Washington University, Ross Hall, Washington, DC, USA
11 Facultad de Medicina Veterinaria y Agronomía, Universidad de Las Américas, sede Providencia, Manuel Montt 948, 7500975, Santiago, Chile
12 Department of Biology, Faculty of Sciences, Universidad de Chile, Santiago, Chile
13 Public Nutrition Unit, Institute for Nutrition and Food Technologies, Universidad de Chile, Santiago, Chile
14 The Buck Institute for Research on Aging, Novato, USA
15 Latin American Brain Health Institute (BrainLat), Universidad Adolfo Ibañez, Santiago, Chile
16 Biomedical Neuroscience Institute and Department of Neurosciences, Faculty of Medicine, Universidad de Chile, Santiago 8380000, Chile
17 Institute for Research in Dental Sciences (ICOD), Faculty of Dentistry, Universidad de Chile, Santiago 8380544, Chile
18 Oficina de apoyo a la investigación clínica, hospital clínico universidad de Chile, Santiago 8380494, Chile
19 Leibniz Institute for Neurobiology, 39118 Magdeburg, Germany
20 Photonscore GmbH, Brenneckestr. 20, 39118 Magdeburg, Germany

*Corresponding author at: Faculty of Medicine, Universidad de los Andes, Santiago 7620001, Chile. aluarte@uandes.cl

Abstract

The regenerative potential of developing cortical axons following injury depends on intrinsic mechanisms, such as axon-autonomous protein synthesis, that are still not fully understood. An emerging factor in this regenerative process is the bi-directional interplay between microtubule dynamics and structural proteins of the axonal endoplasmic reticulum. Therefore, we hypothesize that locally synthesized structural proteins of the endoplasmic reticulum may regulate microtubule dynamics and the outgrowth of injured cortical axons. This hypothesis is supported by RNA data-mining, which identified Reticulon-1 as the sole ER-shaping protein consistently present in axonal transcriptomes and found it to be downregulated following cortical axon injury. Using compartmentalized microfluidic chambers, we demonstrate that local knockdown of Reticulon-1 mRNA enhances outgrowth while reducing the distal tubulin levels of injured cortical axons. Additionally, live cell imaging shows injury-induced reductions in microtubule growth rate and length, which are fully restored by axonal Reticulon-1 knockdown. Interestingly, axonal inhibition of the microtubule-severing protein Spastin fully prevents the effects of local Reticulon-1 knockdown on outgrowth and tubulin levels, while not affecting microtubule dynamics. Furthermore, we provide evidence supporting that the Reticulon-1C isoform is locally synthesized in injured axons and associates with Spastin to inhibit its severing activity. Our findings reveal a novel injury-dependent mechanism in which a locally synthesized ER-shaping protein lessens microtubule dynamics and the outgrowth of cortical axons.

Introduction

Developing cortical axons can regenerate after injury but lose this capacity in adulthood[1]. The regenerative potential of developing axons depends on extrinsic and intrinsic (cell autonomous) factors that regulate their outgrowth[2]. The structure of the axonal endoplasmic reticulum (ER) is a key intrinsic factor for outgrowth during development and post-injury[3–8]. Indeed, locally synthesized proteins of the axonal ER promote regeneration [9–11]. However, the role of axonal protein synthesis in shaping ER function and regeneration after injury remains poorly understood.

Unlike the ribosome-rich somato-dendritic ER, the axonal ER structure predominantly comprises continuous tubules of smooth ER, maintained by specific ER-shaping proteins [12,13]. The axonal ER controls calcium regulation, lipid provision, and transmembrane protein supply, which contribute to axon elongation [14–17]. A bi-directional relationship of the axonal ER with microtubule dynamics has emerged as critical for axon outgrowth. For instance, the physical coupling of the axonal ER to growing microtubules through STIM1 determines its positioning into filopodia in growth cones to control guidance of developing axons [18]. In turn, the axonal ER controls microtubule dynamics, which is required for axonal specification and proper outgrowth in response to injury [7,19].

The interactome of the axonal ER provides relevant information about its control over microtubule dynamics[20,21]. In fact, the interaction of ER structural proteins with those enzymes regulating microtubule severing may contribute to sculpt the axonal cytoskeleton required for outgrowth [22,23]. As such, the microtubule-severing protein Spastin is known to interact with different ER-shaping proteins, [20,21] but the contribution of axonal protein synthesis to this process has not been addressed. Here, we hypothesized that the local synthesis of ER structural proteins control microtubule dynamics, contributing to the elongation of injured axons. Using a variety of techniques, we report that local synthesis of the ER shaping protein Reticulon-1 (Rtn-1) controls microtubule dynamics and the outgrowth of injured cortical axons depending on the activity of the microtubule-severing protein Spastin.

Results

Rtn-1 is consistently present in axonal transcriptomes

As a first approach to test our hypothesis, we looked for mRNAs coding for ER structural proteins in reported transcriptomes from isolated axons of murine and human origin (Table I). To increase the robustness of our analysis, we focused on common transcripts. We identified 104 common mRNAs reported in all these studies (Figure 1A) and classified common mRNAs within the Gene Ontology (GO) category 'Cellular Component' in Gene Ontology (GO) analysis. We found that Rtn-1 mRNA was the only common transcript coding for an ER structural protein (Figure 1B). Furthermore, one of these studies showed that Rtn-1 mRNA levels are decreased by 5.26 ± 0.06-fold in cortical axons after axotomy [24]. Thus, Rtn-1 mRNA is consistently present in intact axons, and it is regulated upon injury.

Next, we studied the distribution of Rtn-1 protein in axons from cultured rat cortical neurons at early developmental stages. Specifically, we assessed the fluorescence intensity of Rtn-1 along the terminal 50 µm of axonal segments at 1, 3, and 7 days *in vitro* (DIV). Axonal identity was confirmed by their positivity for β3-tubulin and negativity for the dendritic marker microtubule-associated protein 2 (MAP2). Rtn-1 fluorescence is significantly concentrated in the most distal 10 µm, the region corresponding to the growth cone (GC), with the most marked elevation occurring at 7 DIV as compared to 1 DIV (S1 A-C). This pattern of Rtn-1 enrichment within GCs diverged from the staining pattern of KDEL, a luminal ER marker, which did not exhibit such progressive accumulation (S1 A-C). We also observed a progressive accumulation of Rtn-1 within axonal growth cones. The distribution of Rtn-1 agrees with prior studies that localized this ER-shaping protein at the base of the GC's hand-like structure, as outlined by the actin cytoskeleton stained with phalloidin [5] (S1 D). This distribution supports a model where Rtn-1, as an ER-shaping protein that sculpts and promote the tubular ER, contributes to the dense network of ER tubules characteristically found in the GCs, an observation well-documented in earlier studies[6]

Axonal synthesis of Rtn-1 lessens outgrowth after injury

We first validated knock down (KD) of Rtn-1 in dissociated cortical neurons (7 DIV) through the analysis of its protein levels by WB [25] [26–28]Neuronal Rtn-1 isoforms expressed in neurons include isoform A (Rtn-1A), comprising 776 amino acids, and isoform C (Rtn-1C) with 208 amino acids. Both isoforms share a highly conserved C-terminal region known as the reticulon homology domain (RHD), differing only in their respective 20 N-terminal amino acids [29–31]. Thus, we transfected cortical neurons with siRNAs targeting RHD (i.e., siRNAs that target

148 all Rtn-1 isoforms) or a control sequence (scrambled, Scr). Forty-eight hours later, samples were
149 analyzed by Western blotting (WB) using a pan-Rtn-1 antibody against the highly conserved RHD
150 region. Two distinct Rtn-1 bands were observed: a higher molecular weight band near 180 kDa,
151 likely representing Rtn-1A [32] ,and a lower band near 24 kDa, corresponding to the apparent
152 molecular weight of Rtn-1C[32,33] (Figure 2A). As expected, siRNAs reduced Rtn-1 for both
153 isoforms when compared to Scr, with siRNA2 demonstrating greater efficacy when quantifying
154 the band of lower molecular weight (Figure 2A). Thus, for all subsequent experiments siRNA2
155 was used to downregulate Rtn-1. Immunofluorescence further revealed a marked decrease in Rtn-
156 1 intensity in the somato-dendritic compartment and axons of dissociated cultured neurons co-
157 transfected with RFP plasmid and siRNA2 (Figure 2B).

158 We then performed KD of Rtn-1 mRNA within axonal (axonal Rtn-1 KD) or somato-
159 dendritic (somatic Rtn-1 KD) compartment in microfluidic chambers. This compartmentalized
160 approach has been previously validated in multiple studies to localla control axonal protein
161 synthesis [26–28] .With this approach, we found that axonal Rtn-1 KD did not alter somatic Rtn-1
162 levels yet elicited a significant decrease in somatic β3-tubulin intensity, which was quantified
163 with the intensity fold change for both proteins compared to Scr (Figure 2C). However, axonal
164 KD led to a significant decrease in Rtn-1 fluorescence intensity within the distal 50 µm of axons
165 compared to controls, which did not occur to β3-tubulin, pointing to a specific effect on Rtn-1
166 synthesis (Figure 2D). This was quantified by comparing the area under curve for the intensity
167 profile of both proteins (Figure 2E). These results support that local synthesis of Rtn-1 can be
168 selectively downregulated in the axonal compartment.

169 To investigate the role of local Rtn-1 synthesis in axonal outgrowth, we subjected cortical
170 axons of 8-day in vitro (DIV) to axotomy by vacuum aspiration in microfluidic chambers.
171 Simultaneously, we performed Rtn-1 KD in either the axonal or somato-dendritic compartments
172 and measured outgrowth twenty-four hours later. We quantified the relative number of axonal
173 intersections at incremental distances from the central grooves. Interestingly, we observed a
174 significant increase in outgrowth (higher number of intersections) within the 400-800 µm and
175 800-1200 µm ranges after axonal Rtn-1 KD compared to Scr (Figure 3A). Furthermore, this
176 response was specific for the axonal compartment, as somatic Rtn-1 KD elicited an effect with an
177 opposite trend (Figure 3A).

178 To further characterize the role of axonally synthesized Rtn-1 in injured axons we
179 assessed the morphology of GCs in the same experimental setting described above . To this end,
180 we used β3-tubulin immune staining and phalloidin incubation to reveal the actin cytoskeleton[34].
181 Axonal Rtn-1 KD did not modify the perimeter and the area of GCs. However, axonal Rtn-1 KD
182 produced GCs characterized by a more elongated and compact actin cytoskeleton, reflected on a
183 significant increase in the elongation ratio (i.e, aspect ratio of the actin outline) and longest
184 shortest path (LSP, which reflects the maximum length of the skeletonized outline of GCs),

185 alongside with a reduced number of filopodia (Figure 3B). In contrast, somatic KD did not affect
186 these morphological parameters, except for an increase in the maximum length (Figure 3 B). This
187 analysis revealed that axonal Rtn-1 KD yielded GCs resembling a spade-like morphology that has
188 been previously related to increased outgrowth [34]
189
190 **Axonal Rtn-1 KD decreases β3-tubulin levels in injured axons**
191
192 For complementing the above-described changes on actin cytoskeleton, we started by
193 delineating the relationship between axonal Rtn-1 KD with the microtubule cytoskeleton. As
194 such, first examined the fluorescence intensity of β3-tubulin and Rtn-1 in microfluidic chambers
195 post-axotomy. Differently from what we observed in intact axons (Figure 2D and E),, axonal
196 Rtn-1 KD did not alter Rtn-1 fluorescence significantly but did induce a notable reduction in β3-
197 tubulin intensity compared to control (Figure 4A). In contrast, siRNA added exclusively to the
198 somatodendritic compartment led to a marked decrease in axonal Rtn-1 fluorescence, supporting
199 the notion that most of Rtn-1 protein originates in the soma (Figure 4B). This treatment also
200 decreased somatic β3-tubulin levels (Figure 4B).
201
202 Consistent with a potential compensatory response of the cell body, axonal Rtn-1
203 knockdown (KD) in injured axons leads to an increase in somatic Rtn-1 fluorescence compared
204 to the control (Figure 4C), which may explain the lack of effect on axonal Rtn-1 levels observed
205 in Figure 4A, potentially countered by somatic protein synthesis. Intriguingly, resembling the
206 increase in somatic Rtn-1, β3-tubulin levels were also elevated in the cell bodies following axonal
207 Rtn-1 KD compared to the control (Figure 4C). In contrast, somatic Rtn-1 KD resulted in a
208 simultaneous and significant reduction in somatic fluorescence for both proteins compared to the
209 control (Figure 4D). Together, these results indicate that after axonal injury, the levels of Rtn-1
210 in the somatic and axonal compartments tend to change in a manner that parallels β3-tubulin,
211 suggesting a potential mechanistic relationship between these two proteins[35]
212
213 **Rtn-1 local synthesis dampens outgrowth by shielding Spastin activity**
214
215 The significant alterations in β3-Tubulin levels after Rtn-1 KD in the context of injury,
216 led us to explore potential Rtn-1 interactors that modify microtubule stability could explain these
217 changes. Notably, a previous study had shown that Rtn-1C directly interacts with the microtubule-
218 severing protein Spastin [36]. Thus, we explored the localization of Spastin and Rtn-1C in distal
219 axons before and after injury, and microtubule dynamics under similar conditions. We also
220 examined the influence of Spastin microtubule severing activity on outgrowth by applying

221 Spastazoline (SPTZ), a selective inhibitor of Spastin's AAA ATPase domain (severing domain)[37],
222 to injured axons in microfluidic chambers.
223 To this end, Using Stimulated Emission Depletion (STED) super-resolution microscopy,
224 we stained both non-injured and injured axons in microfluidic chambers with antibodies targeting
225 Spastin (all isoforms) and Rtn-1C. We discovered that the colocalizing fraction of Spastin with
226 Rtn-1C was significantly increased in injured axons (Figure 5A). This result supports the notion
227 that the interaction of both proteins is potentiated after injury.
228 Next, we aimed at exploring whether the increased outgrowth elicited by axonal Rtn-1
229 KD after injury depends on Spastin's microtubule severing activity. To that effect, we studied
230 the effects of axonal Rtn-1 KD on outgrowth forty-eight hours after axotomy. Axonal application
231 of SPTZ in microfluidic chambers abolished the increase in outgrowth elicited by axonal Rtn-1
232 KD compared to control treatments (DMSO + scrambled, Src), which was quantified as the
233 relative number of axonal intersections in different ranges (Figure 5B). As such, this effect on
234 outgrowth was only significant in the 1000-1500 µm range, where the longest axons prevail
235 (Figure 5C). In addition, local SPTZ application in axons treated with a Scr sequence led to a
236 significant outgrowth increase, specifically in the 0-500, and 500-1000 µm ranges (Figure 5B and
237 C). These results reinforce the idea that Spastin severing activity is critical for the outgrowth
238 control depending on locally synthesized Rtn-1 in injured axons.
239 To substantiate the link between axonal Rtn-1 KD and Spastin's microtubule-severing
240 activity, we monitored changes in the fluorescence intensity of β3-tubulin, Rtn-1C, and Spastin
241 48 hours post-axonal injury. As anticipated in Figure 4, axonal Rtn-1 KD resulted in a notable
242 decrease in β3-tubulin within the distal 50µm of axons, compared to the axonal treatment with
243 controls (Scr and DMSO). However, axonal SPTZ incubation completely abolished the β3-
244 tubulin reduction elicited by local Rtn-1 KD (Figure 5D), while it did not alter Rtn-1C and Spastin
245 levels. When combined with a control siRNA sequence, SPTZ administration showed only a
246 slight tendency to raise β3-tubulin levels, without significantly affecting the levels of Rtn-1C and
247 Spastin (Figure 5D). These observations further confirm that axonal Rtn-1 KD is indeed
248 promoting the severing of microtubules by Spastin.
249 Considering the observed shifts in microtubule content and the Spastin's previously
250 reported role in controlling microtubule stability [38–40], we aimed at quantifying microtubule
251 dynamics. We used live-cell imaging of cortical axons from neurons transfected with a plasmid
252 coding for the microtubule tip-binding protein EB3 fused to the fluorescent construct Emerald
253 (EB3-Emerald), which labels the growing plus-ends of microtubules. Axotomy was performed in
254 transfected neurons at 8 DIV (injured), while another set remained intact (non-injured). Axons
255 were transfected with Rtn-1 KD or Scr, and four hours later treated with DMSO, or Spastazoline
256 (SPTZ). Axons in microfluidic chambers were imaged for EB3-Emerald puncta (comets) forty-
257 four hours later (forty-eight hours in total).

First, we aimed at exploring microtubule dynamics after injury. We uncovered that injured axon treated with Scr and DMSO (controls) exhibited a significant nearly two-fold decrease in both the microtubule growth rate and track-length of comets compared to non-injured axons, without changing in the comet lifetime (Figure 5 E and F). Axonal Rtn-1 KD paired with DMSO treatment only tended to increase both microtubule growth rate and comet track length in non-injured axons (Figure 5 E and F). In a marked contrast, axonal Rtn-1 KD of injured axons significantly elevated these parameters not only restoring, but enhancing them beyond the levels observed in non-injured axons (Figure 5 E and F). Comet lifetime remained constant for both non-injured and injured conditions (Figure 5 F). These results indicate that cortical axons significantly modify their microtubule dynamics in response to injury and that interfering the axonal synthesis of Rtn-1 is pivotal for restoring microtubule growth rate and comet track length post-injury.

To explore the contribution of Spastin activity to the control of microtubule dynamic parameters by axonal Rtn-1 synthesis, the axonal compartment of microfluidic chambers was treated with SPTZ, along with Rtn-1 KD. We observed that the increase of microtubule growth rate elicited by axonal Rtn-1 KD was not significantly modified (Figure 5 E and F). This was consistent across both injured and non-injured axons. However, despite not having a net effect on microtubule growth rate, addition of SPTZ to axonal Rtn-1 KD clearly tended to increase the comet track length and lifetime compared to the rest of the conditions from non-injured and injured neurons (Figure 5F). Further, in injured axons, SPTZ significantly increased comet track length elicited by Rtn-1 KD when compared with controls from non-injured axons (Figure 5F). Similarly, the increase in comet lifetime elicited by SPTZ addition to non-injured axons submitted to Rtn-1 KD was significant when compared to Scr+DMSO and siRNA+ DMSO conditions from injured axons (Figure 5F). Together, these results indicate that axonal Rtn-1 synthesis governs microtubule growth rate and comet track length of injured axons beyond the scope of Spastin microtubule severing activity.

Collectively, these results show that in injured axons Rtn-1 would suppress Spastin's severing function, thereby promoting microtubule integrity. The control of Spastin microtubule severing emerges as crucial for controlling outgrowth, and thus, an effective axonal regeneration. Therefore, we aimed at unraveling the precise mechanisms by which Spastin may relate to Rtn-1C in cortical axons

The reticulon isoform 1C (Rtn-1C) is locally synthesized in cortical axons

We first determined that Rtn-1C isoform mRNA and protein are predominant in cortical axons. To prove this point, we employed a culture technique producing 'neuronballs'. This methodology facilitated the segregation of an axon-rich fraction through mechanical separation

295 from the somato-dendritic structures [41]. The resulting desomatized neuronballs underwent
296 immunofluorescence analysis, with axonal compartments identified via staining for medium
297 chain neurofilament (NF-M), and somato-dendritic compartments marked by microtubule-
298 associated protein 2 (MAP2) (Figure 6A). RNA was then extracted from both the axonal and
299 somato-dendritic fractions for reverse transcription PCR (RT-PCR) analysis. The axonal fraction
300 was verified for purity, evidenced by the absence of amplification for MAP2, Histone H1, and
301 glial fibrillary acidic protein (GFAP) mRNAs, yet positive for β-actin transcript, which is known
302 to be present in axonal compartment (Figure 6A). Specific primers targeting the conserved C-
303 terminal domain were used, resulting in the amplification of Rtn-1 transcripts but not Rtn-1A,
304 suggesting Rtn-1C as the dominant isoform within axons (Figure 6A).

305 We further investigated the molecular composition of the axonal and somato-dendritic
306 fractions by WB. Consistent with sample purity, the axonal fraction exhibited the presence of Tau
307 and β3-tubulin proteins, with no detection of the dendritic marker MAP2 (Figure 6A). For Rtn-1
308 identification, we employed a pan-reticulon antibody targeting the conserved C-terminal reticulon
309 homology domain (RHD). Importantly, the axonal fraction showed exclusivity for the lower
310 molecular weight band, indicative of Rtn-1C presence, mirroring RT-PCR results (Figure 6A).
311 Immunofluorescence analysis of Rtn-1C in cortical axons, prepared in microfluidic chambers,
312 displayed a distribution pattern consistent with that of the pan-reticulon Rtn-1 antibody, as
313 illustrated in Figure 2 (Figure 6B). In contrast, Rtn-1A presence was limited to a small subset of
314 axons, exhibiting a peak of localization near the growth cone base (Figure 6B).

315 As shown in figure 2, we have provided evidence compatible with the axonal synthesis
316 of Rtn-1 in cortical axons. In addition, we show that the predominant mRNA and protein in
317 cortical axons correspond to the Rtn-1C isoform (Figure 6 A and B). However, whether Rtn-1C
318 is indeed locally synthesized in cortical axons has not been proved .To demonstrate the local
319 production of Rtn-1C in axons, we employed a proximity ligation assay integrated with
320 puromycilation (puro-PLA) in cultured cortical neurons within microfluidic chambers [42]. During
321 this assay, we selectively administered a puromycin pulse (15 minutes) to the axonal or somato-
322 dendritic compartments, allowing its covalent incorporation into new polypeptides. This enabled
323 the detection of newly synthesized Rtn-1C peptides through fluorescent signals produced by the
324 nanometric proximity (40 nm) of puromycin and Rtn-1C antibodies (Figure 6C). Positive
325 amplification was observed in the somato-dendritic compartment of microfluidic chambers after
326 local puromycin treatment (Figure 6D, left panel). However, no signal was detected in the cell
327 bodies when puromycin was added to the axonal compartment of microfluidic chamber, showing
328 the effective compartmentalization of this approach (Figure 6D, left panel). In addition, positive
329 signal in the cell bodies was also abrogated when the protein synthesis inhibitor emetine was
330 concomitantly applied with puromycin, further supporting that signals reflect protein
331 synthesis(Figure 6D, left panel). Fluorescent puncta in axons after puromycin treatment in the

332 axonal compartment, absent with emetine, indicated local Rtn-1C synthesis (Figure 6D, right
333 panel). Thus, we have unambiguously demonstrated that Rtn-1C is locally produced in cortical
334 axons.
335
336 **Rtn-1C shields the microtubule severing activity of Spastin**
337
338 We established that Rtn-1C is predominant and locally synthesized in cortical axons.
339 Therefore, we aimed at understanding the functional implications of such compartmentalization
340 in relation to Spastin localization and function, when compared to Rtn-1A. To this end, we first
341 over-expressed in COS-7 cells an RFP-tagged version of the most abundant Spastin isoform
342 during neuronal development (M87). In contrast to the Spastin isoform M1, M87 isoform is
343 soluble and devoid of the ER-shaping membrane domain [43]. Next, this plasmid was concomitantly
344 expressed alongside Rtn-1C-GFP or Rtn-1A-GFP and using GFP alone as a control. For
345 comparing microtubule integrity, we also analyzed non-transfected COS-7 cells from each
346 experimental condition. These cells display a radially orientated array of filamentous structures
347 with tubulin staining, compatible with the normal microtubule organization in basal conditions
348 (Figure 7 A).
349
350 Spastin-RFP displayed a punctate distribution when co-expressed with GFP, indicative
351 of the expected soluble distribution of Spastin, and its potential interaction with endosomal and
352 cytoskeletal components (Figure 7B, upper panels). Of note, this distribution pattern was
353 drastically altered when co-expressed with Rtn-1C-GFP (Figure 7B, middle panels). Potentially
354 reflecting their previously reported direct interaction, Spastin closely followed the reticulon
355 pattern (Figure 7B, middle panels). Conversely, Rtn-1A-GFP showed minimal overlap with
356 Spastin-RFP (Figure 7B, lower pannels). Quantification of protein colocalization by Mander's
357 coefficients substantiated these visual observations (Figure 7C).Intriguingly, the co-expression of
358 Spastin-RFP with Rtn-1C-GFP maintained tubulin levels unaltered when compared to non-
359 transfected cells, contrary to the Rtn-1A-GFP and GFP counterpart (Figure 7 B and C).
360 Furthermore, the filamentous distribution of tubulin was clearly preserved with Spastin-RFP/ Rtn-
361 1C-GFP co-expression, which is a strong indicative of limited severing of microtubule filaments
362 (Figure 7 B, middle panels). Therefore, these results suggest that the tight co-distribution of Rtn-
363 1C with Spastin is associated with dampened microtubule severing activity, which is not observed
364 for Rtn-1A isoform.

365 The examination of the sequences of Rtn-1C and 1A reveals a unique N-terminal variance
366 as the point of differentiation between both isoforms, as they largely share their RHD region
367 (Figure 7D). Considering the limited colocalization of Rtn-1A with Spastin (Figure 7B, lower

368 panels), RHD appears not to be sufficient for their interaction. This observation hints at the
369 exclusive 20 N-terminal amino acids of Rtn-1C as being critical for Spastin binding. We
370 performed *in silico* modeling of the Rtn-1C N-terminal and anticipated its affinity with the
371 microtubule-binding domain (MTBD) of Spastin, showing more favorable interaction energies
372 compared to other domains, such as the endosome and microtubule severing domain (-11.2
373 kcal/mol vs -8,3 kcal/mol, and -10,7 kcal/mol, respectively, Figure 7E). Furthermore, the affinity
374 of a Rtn-1A equivalent region for these domains was also less thermodynamically favored
375 compared to Rtn-1C (Figure 7E). These results are compatible with previous evidence showing
376 that deletion of Spastin's MIT, and most of the MTBD region, abrogates Spastin-Rtn-1C co-
377 precipitation[44]. This suggests that Rtn-1C binding to MTBD is competing with the binding of
378 Spastin to microtubules. Mechanistically, this supposes that this binding prevents the ring
379 conformation around microtubule filaments required for the severing activity of Spastin[45]. This
380 control mechanism would be mostly operative after injury, as we showed that the proximity of
381 Rtn-1C/with Spastin is dramatically increased after axotomy (Figure 5A). This would explain
382 why we did not observed changes in tubulin levels after axonal Rtn-1 KD in non-injured axons.

383 Overall, these findings reveal that Rtn-1C, but not Rtn-1A, closely associates with
384 Spastin, leading to a reduction in microtubule severing activity. This interaction maintains tubulin
385 levels and preserves the filamentous structure of microtubules, which might be crucial for protect
386 axonal integrity in response to injury.
387

Discussion

This study uncovers a mechanism whereby local downregulation on the synthesis of an ER-shaping protein promotes the outgrowth of injured cortical axons. Our results support that this enhancement is dependent on the shielding effect that axonally synthesized Rtn-1C exerts over Spastin microtubule severing and microtubule dynamics. Using this mechanism, cortical neurons may precisely and locally control outgrowth after injury. This finely tuned response after damage is intriguing given that its halting effect on outgrowth may seem, at first sight, detrimental for proper regeneration. However, we may speculate that it is also possible that protecting microtubule stability after injury helps axons to transport other molecular components required for a successful injury repair. In any case, it would be interesting to further explore whether intervening the local synthesis of Rtn-1 offers a potential therapeutic effect to enhance the regeneration of CNS axons by unleashing the shielding effect of Rtn-1C synthesis over Spastin microtubule severing locally in axons.

Control of Rtn-1 synthesis as an adaptive mechanism for axonal injury.

It would also be interesting to further explore whether developing neurons decrease axonal Rtn-1 mRNA as a mechanism to promote outgrowth after damage. For instance, a previous study using axotomized 10 DIV rat cortical neurons in microfluidic chambers found a decrease on Rtn-1 mRNA levels compared to non-injured axons[46]. Currently, it is unknown to what extent a similar mechanism is retained in adult cortical neurons. Likewise, we do not know whether this phenomenon is fully operative *in vivo,* even though the mRNA for Rtn-1 is consistently found *in vitro,* and to a lesser extent *ex vivo*. Of note, Rtn-1 mRNA is dynamically regulated in the axonal translatome of retinal ganglion cells *in vivo*[11], but the functional implications of axonal Rtn-1 synthesis in a more physiological context are yet to be elucidated [59]. Interestingly, growing axonal tips from injured nerves in Lamprey are nearly 13-fold enriched in Spastin mRNA, suggesting that other constituent of our described mechanism may be locally synthesized after injury[47].

The presence of the axonal ER (particularly the smooth ER) is thought to be critical for promoting the regeneration of injured neurites by providing membranes and controlling calcium and microtubule dynamics required for outgrowth [48]. This has been supported by evidence showing the distribution of smooth ER markers, including ER-shaping proteins such as reticulons, REEPs, Atlastin, and Spastin isoforms, preferentially at the distal tip of regenerating neurites [49,50]. Indeed, reticulons share RHD with REEPs, some Spastin isoforms, and atlastins, which makes them suitable to shape the tubular smooth ER [30,51]. Highlighting their functional relevance, forcing the localization of smooth ER into axonal tips by the over-expression of the ER membrane protein protrudin enhances outgrowth of CNS axons[8] . Different studies have shown that the presence of

424 the axonal and smooth ER has been associated with more stable microtubules[52–54]. Our results
425 provide a novel mechanism explaining the role of the axonal ER in the control of microtubule
426 severing and outgrowth after injury, i.e., blocking the activity of microtubule severing proteins
427 such as Spastin.

428 The differential injury response in axonal outgrowth observed after somatic or axonal
429 Rtn-1 KD, emphasizes the unique molecular and structural environments of axons versus cell
430 bodies. This difference might be explained by at least two scenarios. Firstly, we used a Rtn-1
431 siRNA that is directed against the conserved RHD sequence, thus also targeting the Rtn-1A
432 isoform. Rtn-1A does not interact with Spastin and has a N- terminal that recruits other signaling
433 pathways [55]. Therefore, the observed differential response might be due to the predominant
434 presence of Rtn-1C in axons, while both isoforms are present in the cell bodies. Secondly,
435 microtubule severing after Rtn-1 KD might promote outgrowth when coupled to predominantly
436 outward-directed growing filaments that characterize axons, but not with the radial or mixed
437 orientation of microtubules in the cell bodies and dendrites, respectively [56].

438 **The role of Spastin's microtubule severing on outgrowth after injury**

439 Microtubule severases, such as Spastin or Katanin, may increase microtubule mass by
440 producing microtubule internal brakes. Indeed, Spastin can stabilize newly produced microtubule
441 tips, paradoxically yielding a net increase in microtubule mass[57]. As such, Spastin tends to
442 concentrate at the tip of growing microtubules to behave as a dual enzyme that cleaves but also
443 stabilizes them after cutting [58]. Our results are compatible with axonal Rtn-1 KD releasing Spastin
444 molecules to sever more microtubules. This process would generate new microtubule growing
445 seeds with more growing ends, and a net increase on filament mass. It is possible that this increase
446 in microtubule mass yields a larger proportion of less stable or more dynamic microtubules ends,
447 which improves elongation. In agreement with this speculation, inhibition of axonal tyrosine
448 ligase (which favor dynamic microtubule ends) impedes outgrowth in injured axons from dorsal
449 root ganglion[59]. Analogously, PTEN suppresses axonal outgrowth in cultured hippocampal
450 neurons by promoting microtubule detyrosination[60]. Furthermore, when Fidgetin (a severing
451 enzyme of microtubule labile ends) is depleted in neurons, axonal regeneration is improved[61].
452 Thus, the direct measurement of axonal microtubule post-translational modifications in our
453 system remains as in interesting research avenue to complement these findings.

454 Like other studies, we observed that increased axonal outgrowth correlates with dynamic
455 microtubule parameters such as growth rate[62]. However, others have shown that the dynamic
456 properties of microtubules, including microtubule growth rate and track length, can adapt to
457 different outgrowth scenarios, with low capacity to predict axonal extension [63]. Thus, controlling
458 microtubule dynamics seems indeed relevant to promote outgrowth and regeneration, but it is not

459 the only factor that determines the outgrowth capacity of injured axons. The exact mechanisms
460 by which locally synthesized Rtn-1C controls dynamic parameters of microtubules remains
461 unsolved. Other Spastin-independent interactions of Rtn-1 may depend on its presence on the
462 tubular ER, which includes the control of functional contacts with mitochondria and
463 autophagosomes [64,65], but their implications for microtubule dynamics and axonal extension also
464 remain to be solved.

465 Decreasing axonal Rtn-1C translation or increasing Spastin microtubule severing locally
466 in axons are emerging mechanism for promoting injury recovery. For instance, local application
467 of recombinant Spastin together with polyethylene glycol increases recovery after sciatic nerve
468 injury [66]. Furthermore, local augmentation of axonal Spastin by the pharmacological local
469 regulation of 14-3-3 promotes the recovery of spinal cord injury[67] . Indeed, axonal regeneration
470 is particularly sensitive to the absence of Spastin[68]. Similarly, results in drosophila show that
471 Spastin gene dosage is particularly relevant for axonal regenerative response [69] .

472 We observed context-dependent effects of Spastin inhibition in the outgrowth of injured
473 axons. As such, under the axonal Rtn-1 KD condition, axonally applied SPTZ decreases
474 outgrowth, restoring it to basal conditions. Paradoxically, axonally applied SPTZ under control
475 conditions increases outgrowth. These results are compatible with a model in which the increase
476 on microtubule severing produced by axonal Rtn-1 KD is fully obliterated by SPTZ addition.
477 Thus, limited Spastin activity would block the increase on microtubule mass and axonal
478 outgrowth. Conversely, under control conditions, a larger fraction of Spastin will be sequestered
479 by axonally synthesized Rtn-1C. In this case, SPTZ will not only block microtubule severing, but
480 may further promote the concentration of Spastin in microtubule growing tips, which due to its
481 dual action, will yield more stable and larger filaments that promote outgrowth.

482 **Implications for length-dependent axonopathies and injury response**

483 The failure of ER shaping protein-function potentially participates in the etiology of
484 multiple length-dependent axonopaties such as hereditary spastic paraplegias (HSPs) [70]. Here we
485 have described a relevant role for the interaction of Rtn-1C with Spastin, which is the most
486 frequently mutated isoform in HSP [44,71]. As a second point of analysis, most studies performed to
487 understand axonopaties and axonal damage have focused on a "cell-body-centered view" for
488 protein synthesis and ER function. However, increasing evidence supports the relevance of axonal
489 autonomy response to injury or cues from the local brain microenvironment [72–75]. Similarly, our
490 work underscores a highly local injury adaptation, which is in harmony with the astonishing
491 extension of central nervous system's axons[76]. These results may provide understanding of axonal
492 pathologies and injury response with a special focus on the autonomous response of cortical
493 axons.

Materials and Methods

Animals and surgical procedures. Pregnant Sprague-Dawley rats were purchased from the Central Animal Facility at Universidad Catolica de Chile and euthanized in accordance with the the Agencia Nacional de Investigación y Desarrollo de Chile (ANID). The experimental protocol was approved by the Institutional Bioethics of Universidad de los Andes (CEC2022106).

Neuron cell cultures. Cortical neurons were cultured from 18-day Sprague-Dawley embryos similar to previously reported [77]. Dissociated primary cortical neurons were seeded on 12 mm glass coverslips coated with 1 mg/mL poly-L-lysine (Sigma-Aldrich, P4707) with 20,000-30,000 cells. Microfluidic chambers were prepared according to Taylor et al[78]. Chambers harboring axonal and somatic compartment connected with a 750 mm long microgroove were mounted over a squared 25mm glass coverslip previously coated with 0.1 mg/mL poly-D-lysine (Corning, 354210) and 2 μg/mL laminin (Sigma, L2020). Plating medium (MEM (Gibco, 15630080), 10 % horse serum (Gibco, 16050122), 0.6 % D-glucose (Sigma Aldrich, G8769), 0.1 % Glutamax (Gibco, 35050061), 2 % penicillin/0.1 % streptomycin (Life Technologies,15140122) was completely replaced with growth medium (Neurobasal (Gibco, 21103049), 3 % B27 (Gibco, 17504044), 0.1 % Glutamax, penicillin/streptomycin 0.1 %) 24 hours after seeding. 100 μL of fresh growth medium was added with a frequency of 48 hours to the somatic compartment to prevent loss of water. Transfections of the somatic compartment (containing soma, dendrites, and axons) or the axonal compartment (containing only axons) were performed on 7 DIV. Neuron ball cell culture was performed like [41]. Briefly, rat cortices were extracted from E18 embryos. Neurons were suspended on growth medium supplemented with 10 % horse serum. A total amount of 30,000 cells were seeded as hanging drops of 20 μL during 3 days inside the cover of 100 mm dishes, which were previously filled with water to prevent the drops get dried. Floating spheres were gently washed three times to discard non-attached cells and then seeded on poly-L-lysine coated 24 wells culture plate (one per well). Each well contained 400 μL of growth medium without serum and was previously supplemented with cytosine *β*-d-arabinofuranoside hydrochloride (AraC) (1 μM, Sigma-Aldrich, C1768) to prevent glial growth. Neurites were allowed to grow until 7 days after seeding. The periphery of each neuron ball was carefully scraped with a pipette and washed three times with cold PBS to further remove any remaining cell bodies. Cell-body-containing spheres were extracted by vacuum suction using a modified pipette tip (near 1 mm diameter). The axonal fraction was then extracted with a cell scraper and submitted to western blot or RT-PCR analysis.

Immunofluorescence. Cultured neurons, dissociated and in microfluidic chambers, were quickly washed twice with PBS and immediately fixed with 4 % PFA (Sigma Aldrich, P6148) 20 min at

531 room temperature. The same procedure was performed for COS7 cells. To assess growth cone
532 morphology cells were fixed 20 min at room temperature by adding same volume of a 8 % PFA
533 and 22 % sucrose solution in PBS. Cells were washed twice with PBS and incubated with
534 permeabilization solution (0.5 % NP-40 (Abcam, ab142227), 0.5 % w/v Bovine Serum Albumin
535 (Winkler, BM-0150) on PBS); quenching solution (50 mM NH_4Cl on PBS) and blocking solution
536 (0.5 % w/v Bovine Serum Albumin, 10% Fetal Bovine Serum (Sigma Aldrich, F2442), on PBS),
537 each step was performed during 10 min at room temperature. Primary antibodies diluted with 0.5
538 % w/v Bovine Serum were incubated overnight at 4º C. The same solution was used to wash the
539 coverslips three times (5 min each) and to dilute secondary antibodies. Secondary antibodies were
540 incubated 1 hour at room temperature. Samples were washed with PBS and distilled water and
541 then mounted using VECTASHIELD®.
542
543 **Colocalization analysis.** Analysis of colocalization was performed as previously described 73.
544 Briefly, samples were acquired on a confocal microscope (Fluoview FV1000) using a UPLSAPO
545 60 x/1.35 NA objective, 4x digital zoom and filtered twice with a Kalman algorithm. An average
546 of 10 confocal images per sample were considered in the analysis (0.2 µm thickness each). We
547 guaranteed that images did not saturate, and that image background was slightly above zero.
548 Image stacks were deconvolved with Huygens Scripting Software (SVI, Hilversum, The
549 Nertherlands) using an algorithm based on the classic maximum likelihood estimator (CMLE).
550 The signal-to-noise ratio was adjusted until the deconvolved images were free of pixel noise.
551 Images were segmented using IDL Workbech 7.0 (ITT Visual Information Solutions, USA).
552 Alternatively, channels were segmented using a series of ImageJ software filters to obtain masked
553 images with JaCoP plugin to simplify the analysis of in vitro experiments. The ratio of
554 colocalization between two signals was calculated using Mander's coefficients and a confined
555 displacement algorithm that determines true and random colocalization. As a result, Mander's
556 coefficients, M1 and M2, were expressed as percentage of true colocalization. For colocalization
557 analysis of Reticulon 1C and Spastin, images were acquired at the Leibniz-Institut für
558 Neurobiologie (LIN, Magdeburg, Germany) using a Leica TCS SP8-3X STED microscope system
559 (Leica Microsystems) equipped with a HC APO CS2 100x/1.40 oil objective. Images were
560 digitalized in 1024 × 1024 pixels format file with 5x zoom factor. These settings achieved an
561 18.93nm resolution in the XY axis and a 220nm resolution in Z. Deconvolution for all images
562 was also performed using the Huygens Scripting Program. Colocalization analysis was then
563 performed using ImageJ JaCoP plugin on 4 confocal slices from each sample, where the axonal
564 cone was present. For this analysis, we used both Reticulon 1C and Spastin STED Channels to
565 estimate both M1 and M2 Mander's coefficients.
566

567 **Fluorescence intensity analysis of somas and axons.** Images were acquired in an Olympus
568 BX61WI microscope equipped with DSU Spinning Disk Confocal System (Photometrics,
569 Tucson, Arizona) and a CCD camera Hamamatsu ORCA-R^2 controlled by the Cell^R software
570 (Olympus, Tokyo, Japan). Axons were randomly imaged with and 40X/1.3 oil immersion
571 objective. Same acquisition parameters were used for all samples on any given condition. To
572 quantify soma intensity, cell bodies were manually segmented following β3-tubulin to determine
573 mean intensity. For all the cells the mean background intensity was subtracted to each cell's mean
574 intensity and the result was multiplied for the corresponding cell area to obtain total intensity. The
575 intensity foldchange was calculated for each cell by dividing its total intensity value by the
576 average of the total intensity from the cells of a given control condition. For axon analysis, 10-30
577 axons were analyzed from at least two microfluidic chambers per experimental condition. For
578 each axon the intensity profile was determined by tracing a 50 μm line (1 μm width) along the
579 axons from their tip depicted by β3-tubulin staining using segmented line tool from FIJI software.
580 For each image an area with no axons was selected to measure mean background fluorescence
581 intensity, which was subtracted to the mean fluorescence intensity value of the corresponding
582 staining. To plot and analyze the differences in the fluorescence intensity after RNAi, the first
583 value of the β3-tubulin average pixel intensity profile was subtracted to all the measurements
584 from each axon. For the analysis of Rtn-1 fluorescence intensity, the average pixel intensity of
585 the last 5 μm was subtracted to all the measurements from each axon. Thus, the corrected values
586 for each channel from a given experimental condition were pooled together from at least three
587 independent cultures.
588
589 **Transfections.** All transfections were performed with lipofectamine 3000 (Thermo Fisher,
590 L3000001) following manufacturer's instructions but without using p3000 reagent. For neurons,
591 RNA or DNA complexes were added to chambers diluted on Neurobasal medium to a total
592 volume of 50 μL per microfluidic chambers or 100 μL for dissociated cultures on 12mm
593 coverslips. For axonal transfection of siRNAs, medium on the axonal compartment was
594 completely removed and replaced with 50 μL of the transfection mixture containing 20pmol of
595 the corresponding oligonucleotide. Near 300 μL of conditioned medium remained at the somatic
596 compartment, generating positive flux towards the axons. By the opposite, for somatic
597 transfection the medium present at the somatic compartment was removed and replaced with 50
598 μL of the transfection mixture, this time generating positive flux towards the soma. For validating
599 siRNA efficiency, 200,000 neurons were seeded on 35 mm plates and transfected with 40 pmol
600 of corresponding oligos and submitted to western blot. A similar procedure was performed with
601 COS7 cells.
602

603 **Axotomy and outgrowth measurement.** Axons were removed from microfluidic chambers of 8
604 DIV by vacuum aspiration with a Pasteur pipette by quickly and repeatedly (5-7 times) aspiring
605 culture medium and replacing it with Neurobasal. Afterward, all Neurobasal was removed and 50
606 μL of the transfection mixture was added either to the axonal or to somatic compartment. To
607 quantify outgrowth images of β3-tubulin staining on axons were binarized and manually
608 segmented to completely follow the shape of axons. A linear profile quantifying the number of
609 intersections for each pixel after the groove (equivalent to 1200 μm or 1500 μm) was obtained.
610 Different axonal fields were measured an averaged on each date from at least two microfluidic
611 chambers per condition. To obtain the relative number of intersections, values obtained from each
612 field were normalized by the total number of intersections of the first pixel.
613
614 **Probe-labeling of primary antibodies for PLA.** Monoclonal antibodies Mouse anti-reticulon-
615 1C and mouse anti-puromycin (3RH1, Kerafast) were directly labeled with the Duolink® In Situ
616 Probemaker PLUS (1002748995, Sigma Aldrich) and MINUS (1002748992, Sigma Aldrich),
617 respectively, following manufacturer`s instructions. Both antibodies with a concentration of 1
618 μg/μL were labeled overnight at room temperature with the corresponding buffer and probes to a
619 final volume of 20 μL. Labeled antibodies were further diluted with 20 μL of storage solution.
620
621 **Puro-PLA staining protocol.** Puro-PLA was performed on similar conditions to well stablished
622 protocols [42]. Briefly, puromycin (1.8 μM, P8833, Sigma-Aldrich) or pure growth medium
623 without puromycin (negative control) was added exclusively to the axonal or somatic
624 compartment on microfluidic chambers with 9 div cortical cells during 15 minutes. As an
625 additional negative control, this incubation step was performed on the presence of emetin (40
626 nM, E2375, Sigma-Aldrich) either on somatic or axonal compartment when stated. To
627 completely block protein synthesis, emetin incubation was performed 90 minutes before
628 puromycin addition to the corresponding compartment. Immediately after incubations, cells
629 were washed twice witmn h PBS and fixed with 4 % paraformaldehyde and 4 % sucrose on
630 PBS for 20 min at room temperature; washed again three times with PBS for 5 min and
631 permeabilized 10 min with 0.25 % Triton X-100 on PBS. After permeabilization, cells were
632 washed three times with PBS for 5 MIN; blocked with 5 % Goat serum on PBS for 1 hour and
633 incubated with the probe-labeled antibodies (labeled anti-reticulon-1C 1: 50 and labeled anti-
634 puromycin 1:200) overnight in the same solution at 4º C. Detection of locally synthesized
635 reticulon-1C was perform under manufacturer`s instructions, but without the step of labeled
636 secondary antibodies. Cells were further incubated 1 hour at room temperature with anti-β3-
637 tubulin conjugated to Alexa Fluor 488 and then mounted with the Duolink In Situ Mounting
638 Medium with DAPI (Sigma-Aldrich). Pictures were acquired as previously described using a

639 Zeiss LSM 800 confocal microscope, using a 63x oil objective and PLA positive puncta
640 present on a mask for -β3-tubulin were quantified with FIJI software. At least five axonal or
641 somatic fields were analyzed from each chamber.
642
643 **RT-PCR.** For axonal RNA isolation at least 200 neuron balls were desomatized and removed by
644 using lysis buffer provided by the RNAqueous™-Micro Total RNA Isolation Kit (AM193,
645 ThermoFisher) followed by the manufacture's protocol. Total RNA was eluted twice to a volume
646 of 30µL. Approximately 20-30 axotomized neuron balls were submitted to the same protocol and
647 RNA was also resuspended on 30µL. Reverse transctiption was carried out by using 100 ng as
648 starting material with the High-Capacity cDNA Reverse Transcription Kit (4368814, Thermo
649 Fisher) and the products were DNAse treated under manufacturer`s instructions (EN0521,
650 Thermo Fisher). For the PCR 3 µL of cDNA products were amplified using GoTaq® Green
651 Master Mix, 2X (M712, Promega) with the following protocol: a denaturing step at 95º C for 5
652 min, 35 cycles of denaturation at 95º C for 30 s, extension at 57º C for 30 sec and 72º C for 45
653 sec, at the end of the cycles temperature was kept at 72º C for 10 min. Afterward, 10 µL of the
654 solution containing the amplified sequences were loaded into a 2 % agarose gel and stained with
655 GelRed® Nucleic Acid Gel Stain (Biotum, 41003) under manufacturer´s instructions.
656
657 **Western blot.** For protein isolation RIPA buffer (50 mM Tris-HCl, pH 7.4, 150 mM NaCl, 0.25
658 % deoxycholic acid, 1 % NP-40, 1 % SDS, 1 mM EDTA, supplemented with protease and
659 phosphatase inhibitors (Thermo Fisher, A32963). Extracted proteins were quantified by the
660 Bicinchoninic Acid method (BCA, Thermo Fisher, 23225) and separated by polyacrylamide gels
661 under denaturant conditions SDS-PAGE[79]. 20 µg of protein was loaded per lane for all complete
662 neuronal homogenates and for the axonal and somatic fraction of neuron balls. Linear acrylamide
663 gels 15 % w / v, electrophoresis was performed at 70 V for 45 min, and 45 min at 100 V. The
664 transfer of proteins from the gel to a membrane Nitrocellulose (BioRad) was performed with a
665 constant current of 350 mA for 90 min. After transference, membranes were blocked with 5 %
666 w/v skim milk in PBS for 1 h at room temperature under constant agitation. Then, membranes
667 were incubated at 4° C with the corresponding antibody diluted in PBS with constant shaking
668 over-night. The next day, membranes were incubated with the corresponding secondary antibody
669 for 1 h at room temperature. Bands were quantified by densitometry using the program Photoshop
670 7.0 (Adobe).
671
672 **Live imaging of EB3-Emerald microtubule plus-ends.** Neurons were cultured on microfluidic
673 chambers and transfected with EB3-Emerald plasmid at day *in vitro* 7. Neurons were axotomized
674 by vacuum aspiring at 8 DIV and transfected with the corresponding siRNA in the axonal

675 compartment. Spastin inhibitor (Spastazoline, HY-111548, Medchemexpress) was added to the
676 axonal compartment 4-5 hours after the transfection of the corresponding oligos. Axons were
677 imaged in the microfluidic chamber after axotomy. EB3-Emerald transfected axons were
678 randomly selected and imaged at 32ºC in tyrode's solution (125 mM NaCl, 2 mM KCl, 2 mM
679 $CaCl_2$, 2 mM $MgCl_2$, 30 mM glucose, 25 mM HEPES, pH 7.4) for 3 min with an acquisition of 2
680 frames per sec. Cells were let to equilibrate for 10 minutes before measurements and a difference
681 in the volume between compartments of at least 100 μL was always kept in order to maintain the
682 hydrostatic pressure towards the axons. The experiment was acquired at 2 frames per second with
683 an inverted microscope (Observer. D1; Zeiss) equipped with an EMCCD camera (Evolve 512;
684 Delta Photometrics) operated by VisiView® Software (Visitron Systems GmbH). A 63x
685 objective and GFP single band exciters ET filter set (excitation 470/40, emission 59022m,
686 dichroic 59022BS) were used. mEmerald-EB3-C-20 was a gift from Michael Davidson (Addgene
687 plasmid # 54076 ; http://n2t.net/addgene:54076 ; RRID:Addgene_54076)
688
689 **Analysis of microtubule dynamics.** All the acquired time series were filtered with Gaussian blur
690 3D function from FIJI software. Mobile components of the image series were captured by
691 applying a 4 sigma Gaussian blur, while more static elements were captured by applying a 50
692 sigma filter processing similar to . To improve movement detection, static elements were
693 subtracted from mobile components with the function "image calculator" from FIJI. The filtered
694 image series were used to construct kymographs with the plugin "kymograph builder" of FIJI. All
695 kymographs were constructed from the more distal portion of axons by tracing a line of one
696 micrometer width with a total length ranging from 30 to 50 um. Growth cones were not included
697 in the analysis. All the analyzed parameters were calculated like previously described [80]. EB3-
698 Emerald dashes on the kymographs were manually traced with a straight line and their velocity
699 were calculated by dividing the displacement of a dash (microtubule growth rate) and the total
700 time spent travelling (microtubule lifetime), microtubule track length was obtained by dividing.
701 The parameter "total number of comets" was obtained by counting the number of dashes in one
702 kymograph and dividing this value by the total length. Only dashes that could be followed by two
703 consecutive frames were considered for all the analyses.
704
705 **Molecular docking between Spastin M87 and Rtn-1C**. Firstly, spastin M1 and Rtn-1A models
706 of rattus norvegicus were retrieved from AlphaFold Protein Structure Database (accession
707 numbers AF-A0A0G2K590 and AF-Q64548, respectively). Then, M87 spastin model were
708 generated from the removal of the first 86 amino acids of the M1 spastin model, whereas Rtn-1C
709 3D-structure was built with MODELLER version 10.4 using Rtn-1A model as template. For this,
710 amino acid sequences of Rtn-1C were retrieved from UniprotKB/Swissprot (accession numbers
711 Q64548). Additionally, the first 20 amino acids (of the N-terminal region) of the Rtn-1C model

712 and region 200-317 containing the "microtubule-binding" domain of spastin M87 were refined
713 using ModLoop server (Fiser & Sali, 2003). Subsequently, we evaluated the interaction of the
714 Rtn-1C N-terminal with three domains of spastin M87 - endosome o MIT (region 116-194),
715 microtubule-binding (region 270-328) and microtubule-severing o AAA ATPase (region 342-
716 599) - using the HADDOCK docking protein-protein web server[81]. Among many models, low-
717 energy conformations for each complex were extracted from HADDOCK 2.2 server, as
718 previously described[82] The binding energy (ΔG_{bin}) of the complexes were predicted using the
719 PRODIGY web server at temperature of 310 K, and chains identifiers for Rtn-1 and spastin M87
720 were specified as Interactor 1 and 2, respectively. Finally, graphical analysis of molecular docking
721 studies was performed using VMD 1.9.2 software[83] .
722
723 **Statistical Analysis** Results are expressed as mean ± SEM. Data were analyzed using the
724 Shapiro–Wilk normality test to determine the appropriate statistical method. For normally
725 distributed data, Student's t-test was performed when comparing two groups or Mann-Whitney U
726 test for non-parametric data. Multiple group comparisons were conducted using one-way
727 ANOVA followed by Tukey's post hoc test. For non-normally distributed data, the Wilcoxon
728 signed-rank test was used. Statistical significance was defined as a P value <0.05
729

References

Cooke, P., Janowitz, H. & Dougherty, S. E. Neuronal Redevelopment and the Regeneration of Neuromodulatory Axons in the Adult Mammalian Central Nervous System. *Front Cell Neurosci* **16**, 872501 (2022).

He, Z. & Jin, Y. Intrinsic Control of Axon Regeneration. *Neuron* **90**, 437–451 (2016).

Aridor, M. & Fish, K. N. Selective Targeting of ER Exit Sites Supports Axon Development. *Traffic* **10**, 1669–1684 (2009).

Krijnse-Locker, J., Parton, R. G., Fuller, S. D., Griffiths, G. & Dotti, C. G. The organization of the endoplasmic reticulum and the intermediate compartment in cultured rat hippocampal neurons. *Mol Biol Cell* **6**, 1315–32 (1995).

Nozumi, M. *et al.* Identification of functional marker proteins in the mammalian growth cone. *Proc Natl Acad Sci U S A* **106**, 17211–6 (2009).

Deitch, J. S. & Banker, G. A. An electron microscopic analysis of hippocampal neurons developing in culture: early stages in the emergence of polarity. *J Neurosci* **13**, 4301–15 (1993).

Rao, K. *et al.* Spastin, atlastin, and ER relocalization are involved in axon but not dendrite regeneration. *Mol Biol Cell* (2016) doi:10.1091/mbc.E16-05-0287.

Petrova, V. *et al.* Protrudin functions from the endoplasmic reticulum to support axon regeneration in the adult CNS. *Nature Communications 2020 11:1* **11**, 1–15 (2020).

Pacheco, A., Merianda, T. T., Twiss, J. L. & Gallo, G. Mechanism and role of the intra-axonal Calreticulin translation in response to axonal injury. *Exp Neurol* (2020) doi:10.1016/j.expneurol.2019.113072.

Willis, D. *et al.* Differential transport and local translation of cytoskeletal, injury-response, and neurodegeneration protein mRNAs in axons. *Journal of Neuroscience* (2005) doi:10.1523/JNEUROSCI.4235-04.2005.

Shigeoka, T. *et al.* Dynamic Axonal Translation in Developing and Mature Visual Circuits. *Cell* **166**, 181–192 (2016).

Wu, Y. *et al.* Contacts between the endoplasmic reticulum and other membranes in neurons. *Proc Natl Acad Sci U S A* (2017) doi:10.1073/pnas.1701078114.

Voeltz, G. K., Prinz, W. A., Shibata, Y., Rist, J. M. & Rapoport, T. A. A class of membrane proteins shaping the tubular endoplasmic reticulum. *Cell* **124**, 573–86 (2006).

Luarte, A., Cornejo, V. H., Bertin, F., Gallardo, J. & Couve, A. The axonal endoplasmic reticulum: One organelle—many functions in development, maintenance, and plasticity. *Developmental Neurobiology* Preprint at https://doi.org/10.1002/dneu.22560 (2018).

González, C. *et al.* Axons provide the secretory machinery for trafficking of voltage-gated sodium channels in peripheral nerve. *Proc Natl Acad Sci U S A* **113**, 1823–1828 (2016).

Cornejo, V. H., Luarte, A. & Couve, A. Global and local mechanisms sustain axonal proteostasis of transmembrane proteins. *Traffic* **18**, 255–266 (2017).

de Juan-Sanz, J. *et al.* Axonal Endoplasmic Reticulum Ca2+ Content Controls Release Probability in CNS Nerve Terminals. *Neuron* **93**, 867-881.e6 (2017).

Pavez, M. *et al.* STIM1 is required for remodeling of the endoplasmic reticulum and microtubule cytoskeleton in steering growth cones. *Journal of Neuroscience* (2019) doi:10.1523/JNEUROSCI.2496-18.2019.

Farías, G. G. *et al.* Feedback-Driven Mechanisms between Microtubules and the Endoplasmic Reticulum Instruct Neuronal Polarity. *Neuron* (2019) doi:10.1016/j.neuron.2019.01.030.

Evans, K. *et al.* Interaction of two hereditary spastic paraplegia gene products, spastin and atlastin, suggests a common pathway for axonal maintenance. *Proc Natl Acad Sci U S A* (2006) doi:10.1073/pnas.0510863103.

Mannan, A. U. *et al.* Spastin, the most commonly mutated protein in hereditary spastic paraplegia interacts with Reticulon 1 an endoplasmic reticulum protein. *Neurogenetics* (2006) doi:10.1007/s10048-006-0034-4.

Stone, M. C. *et al.* Normal Spastin Gene Dosage Is Specifically Required for Axon Regeneration. *Cell Rep* **2**, 1340–1350 (2012).

Rao, K. *et al.* Spastin, atlastin, and ER relocalization are involved in axon but not dendrite regeneration. *Mol Biol Cell* (2016) doi:10.1091/mbc.E16-05-0287.

Taylor, A. M. *et al.* Axonal mRNA in Uninjured and Regenerating Cortical Mammalian Axons. *Journal of Neuroscience* **29**, 4697–4707 (2009).

Hengst, U., Cox, L. J., Macosko, E. Z. & Jaffrey, S. R. Functional and selective RNA interference in developing axons and growth cones. *Journal of Neuroscience* (2006) doi:10.1523/JNEUROSCI.5229-05.2006.

Baleriola, J. *et al.* Axonally synthesized ATF4 transmits a neurodegenerative signal across brain regions. *Cell* **158**, 1159–1172 (2014).

Batista, A. F. R., Martínez, J. C. & Hengst, U. Intra-axonal Synthesis of SNAP25 Is Required for the Formation of Presynaptic Terminals. *Cell Rep* (2017) doi:10.1016/j.celrep.2017.08.097.

Zhang, Y. *et al.* The MicroRNA-17-92 cluster enhances axonal outgrowth in embryonic cortical neurons. *J Neurosci* **33**, 6885–94 (2013).

Van De Velde, H. J. K., Roebroek, A. J. M., Senden, N. H. M., Ramaekers, F. C. S. & Van De Ven, W. J. M. NSP-encoded reticulons, neuroendocrine proteins of a novel gene family associated with membranes of the endoplasmic reticulum. *J Cell Sci* **107**, 2403–2416 (1994).

Chiurchiù, V., Maccarrone, M. & Orlacchio, A. The role of reticulons in neurodegenerative diseases. *Neuromolecular Med* **16**, 3–15 (2014).

Roebroek, A. J. M. *et al.* Cloning and expression of alternative transcripts of a novel neuroendocrine-specific gene and identification of its 135-kDa translational product. *Journal of Biological Chemistry* **268**, 13439–13447 (1993).

Van De Velde, H. J. K., Roebroek, A. J. M., Senden, N. H. M., Ramaekers, F. C. S. & Van De Ven, W. J. M. NSP-encoded reticulons, neuroendocrine proteins of a novel gene family associated with membranes of the endoplasmic reticulum. *J Cell Sci* **107**, 2403–2416 (1994).

Roebroek, A. J. M. *et al.* Cloning and expression of alternative transcripts of a novel neuroendocrine-specific gene and identification of its 135-kDa translational product. *Journal of Biological Chemistry* **268**, 13439–13447 (1993).

Kaethner, R. J. & Stuermer, C. A. 0. Dynamics of Terminal Arbor Formation and Target Approach of Retinotectal Axons in Living Zebrafish Embryos: A Time-Lapse Study of Single Axons. *The Journal of Neuroscience* **72**, 32573271 (1992).

Fan, X. xuan *et al.* Knockdown of RTN1-C attenuates traumatic neuronal injury through regulating intracellular Ca2+ homeostasis. *Neurochem Int* **121**, 19–25 (2018).

Mannan, A. U. *et al.* Spastin, the most commonly mutated protein in hereditary spastic paraplegia interacts with Reticulon 1 an endoplasmic reticulum protein. *Neurogenetics* **7**, 93–103 (2006).

Cupido, T., Pisa, R., Kelley, M. E. & Kapoor, T. M. Designing a chemical inhibitor of the AAA protein spastin using active site mutations. *Nat Chem Biol* **15**, 444 (2019).

Teixeira Lopes, A. Spastin regulates microtubule dynamics and is required for normal motor and cognitive functions. (2018).

Aiken, J. & Holzbaur, E. L. F. Spastin locally amplifies microtubule dynamics to pattern the axon for presynaptic cargo delivery. *bioRxiv* **123**, 332a (2024).

Kuo, Y. W., Trottier, O., Mahamdeh, M. & Howard, J. Spastin is a dual-function enzyme that severs microtubules and promotes their regrowth to increase the number and mass of microtubules. *Proc Natl Acad Sci U S A* **116**, 5533–5541 (2019).

Sasaki, Y. *et al.* Phosphorylation of Zipcode Binding Protein 1 Is Required for Brain-Derived Neurotrophic Factor Signaling of Local -Actin Synthesis and Growth Cone Turning. *Journal of Neuroscience* **30**, 9349–9358 (2010).

Dieck, S. tom *et al.* Direct visualization of identified and newly synthesized proteins in situ. *Nat Methods* (2015) doi:10.1038/nmeth.3319.

Solowska, J. M., Rao, A. N. & Baas, P. W. Truncating mutations of SPAST associated with hereditary spastic paraplegia indicate greater accumulation and toxicity of the M1 isoform of spastin. *Mol Biol Cell* **28**, 1728 (2017).

Mannan, A. U. *et al.* Spastin, the most commonly mutated protein in hereditary spastic paraplegia interacts with Reticulon 1 an endoplasmic reticulum protein. *Neurogenetics* **7**, 93–103 (2006).

Roll-Mecak, A. & Vale, R. D. Structural basis of microtubule severing by the hereditary spastic paraplegia protein spastin. *Nature* (2008) doi:10.1038/nature06482.

Taylor, A. M. *et al.* Axonal mRNA in Uninjured and Regenerating Cortical Mammalian Axons. *The Journal of Neuroscience* **29**, 4697 (2009).

Jin, L. Q. *et al.* Transcriptomes of Injured Lamprey Axon Tips: Single-Cell RNA-Seq Suggests Differential Involvement of MAPK Signaling Pathways in Axon Retraction and Regeneration after Spinal Cord Injury. *Cells* **11**, 2320 (2022).

Luarte, A., Cornejo, V. H., Bertin, F., Gallardo, J. & Couve, A. The axonal endoplasmic reticulum: One organelle—many functions in development, maintenance, and plasticity. *Developmental Neurobiology* Preprint at https://doi.org/10.1002/dneu.22560 (2018).

Rao, K. *et al.* Spastin, atlastin, and ER relocalization are involved in axon but not dendrite regeneration. *Mol Biol Cell* (2016) doi:10.1091/mbc.E16-05-0287.
Stone, M. C. *et al.* Normal Spastin Gene Dosage Is Specifically Required for Axon Regeneration. *Cell Rep* **2**, 1340–1350 (2012).
Iwahashi, J., Hamada, N. & Watanabe, H. Two hydrophobic segments of the RTN1 family determine the ER localization and retention. *Biochem Biophys Res Commun* **355**, 508–512 (2007).
Farías, G. G. *et al.* Feedback-Driven Mechanisms between Microtubules and the Endoplasmic Reticulum Instruct Neuronal Polarity. *Neuron* (2019) doi:10.1016/j.neuron.2019.01.030.
Rao, K. *et al.* Spastin, atlastin, and ER relocalization are involved in axon but not dendrite regeneration. *Mol Biol Cell* (2016) doi:10.1091/mbc.E16-05-0287.
Lee, M. *et al.* Drosophila Atlastin regulates the stability of muscle microtubules and is required for synapse development. *Dev Biol* **330**, 250–262 (2009).
Kaya, L. *et al.* Direct association of the reticulon protein RTN1A with the ryanodine receptor 2 in neurons. *Biochim Biophys Acta* **1833**, 1421 (2013).
Baas, P. W., Rao, A. N., Matamoros, A. J. & Leo, L. Stability properties of neuronal microtubules. *Cytoskeleton (Hoboken)* **73**, 442 (2016).
Kuo, Y. W. & Howard, J. Cutting, Amplifying, and Aligning Microtubules with Severing Enzymes. *Trends Cell Biol* **31**, 50 (2021).
Kuo, Y. W., Trottier, O., Mahamdeh, M. & Howard, J. Spastin is a dual-function enzyme that severs microtubules and promotes their regrowth to increase the number and mass of microtubules. *Proc Natl Acad Sci U S A* **116**, 5533–5541 (2019).
Song, W., Cho, Y., Watt, D. & Cavalli, V. Tubulin-tyrosine ligase (TTL)-mediated increase in tyrosinated α-tubulin in injured axons is required for retrograde injury signaling and axon regeneration. *Journal of Biological Chemistry* **290**, 14765–14775 (2015).
Kath, C. *et al.* PTEN suppresses axon outgrowth by down-regulating the level of detyrosinated microtubules. (2018) doi:10.1371/journal.pone.0193257.
Matamoros, A. J. *et al.* Knockdown of Fidgetin Improves Regeneration of Injured Axons by a Microtubule-Based Mechanism. *Journal of Neuroscience* **39**, 2011–2024 (2019).
Liz, M. A. *et al.* Neuronal deletion of GSK3β increases microtubule speed in the growth cone and enhances axon regeneration via CRMP-2 and independently of MAP1B and CLASP2. *BMC Biol* **12**, 1–19 (2014).
Kiss, A., Fischer, I., Kleele, T., Misgeld, T. & Propst, F. Neuronal growth cone size-dependent and -independent parameters of microtubule polymerization. *Front Cell Neurosci* **12**, 195 (2018).
D' Eletto, M. *et al.* Modulation of autophagy by RTN-1C: role in autophagosome biogenesis. *Cell Death Dis* **10**, (2019).
Reali, V. *et al.* Reticulon protein-1C is a key component of MAMs. *Biochim Biophys Acta* **1853**, 733–745 (2015).
Lin, Y. F. *et al.* Effect of exogenous spastin combined with polyethylene glycol on sciatic nerve injury. *Neural Regen Res* **14**, 1271–1279 (2019).
Liu, Q. *et al.* 14-3-3 protein augments the protein stability of phosphorylated spastin and promotes the recovery of spinal cord injury through its agonist intervention. *Elife* **12**, (2024).
Stone, M. C. *et al.* Normal Spastin Gene Dosage Is Specifically Required for Axon Regeneration. *Cell Rep* **2**, 1340–1350 (2012).
Stone, M. C. *et al.* Normal spastin gene dosage is specifically required for axon regeneration. *Cell Rep* **2**, 1340–1350 (2012).
Blackstone, C., Kane, C. J. O., Reid, E., O'Kane, C. J. & Reid, E. Hereditary spastic paraplegias: membrane traffic and the motor pathway. *Nat Rev Neurosci* **12**, 31–42 (2011).
Hazan, J. *et al.* Spastin, a new AAA protein, is altered in the most frequent form of autosomal dominant spastic paraplegia. *Nat Genet* **23**, 296–303 (1999).
Zhang, Y. *et al.* The MicroRNA-17–92 Cluster Enhances Axonal Outgrowth in Embryonic Cortical Neurons. *Journal of Neuroscience* **33**, 6885–6894 (2013).
Zhang, Y. *et al.* MicroRNAs in the axon locally mediate the effects of chondroitin sulfate proteoglycans and cGMP on axonal growth. *Dev Neurobiol* **75**, 1402–1419 (2015).
Lopez-Verrilli, M. A., Picou, F. & Court, F. A. Schwann cell-derived exosomes enhance axonal regeneration in the peripheral nervous system. *Glia* (2013) doi:10.1002/glia.22558.
Jung, H., Gkogkas, C. G., Sonenberg, N. & Holt, C. E. Remote control of gene function by local translation. *Cell* Preprint at https://doi.org/10.1016/j.cell.2014.03.005 (2014).
Lin, H.-M. *et al.* Reconstruction of Intratelencephalic Neurons in the Mouse Secondary Motor Cortex Reveals the Diverse Projection Patterns of Single Neurons. *Front Neuroanat* **12**, (2018).

Deitch, J. S. & Banker, G. A. An electron microscopic analysis of hippocampal neurons developing in culture: early stages in the emergence of polarity. *J Neurosci* **13**, 4301–15 (1993).
Taylor, A. M. *et al.* A microfluidic culture platform for CNS axonal injury, regeneration and transport. *Nat Methods* (2005) doi:10.1038/nmeth777.
Cleveland, D. W., Fischer, S. G. & Kirschner andLaemmli, M. W. U. K. Peptide mapping by limited proteolysis in sodium dodecyl sulfate and analysis by gel electrophoresis. *Journal of Biological Chemistry* **252**, 1102–1106 (1977).
Stepanova, T. *et al.* History-dependent catastrophes regulate axonal microtubule behavior. *Current Biology* (2010) doi:10.1016/j.cub.2010.04.024.
Van Zundert, G. C. P. *et al.* The HADDOCK2.2 Web Server: User-Friendly Integrative Modeling of Biomolecular Complexes. *J Mol Biol* **428**, 720–725 (2016).
Acevedo, W., Ramírez-Sarmiento, C. A. & Agosin, E. Identifying the interactions between natural, non-caloric sweeteners and the human sweet receptor by molecular docking. *Food Chem* **264**, 164–171 (2018).
Humphrey, W., Dalke, A. & Schulten, K. VMD: Visual molecular dynamics. *J Mol Graph* **14**, 33–38 (1996).
Saal, L., Briese, M., Kneitz, S., Glinka, M. & Sendtner, M. Subcellular transcriptome alterations in a cell culture model of spinal muscular atrophy point to widespread defects in axonal growth and presynaptic differentiation. *RNA* **20**, 1789–1802 (2014).
Rotem, N. *et al.* ALS Along the Axons - Expression of Coding and Noncoding RNA Differs in Axons of ALS models. *Sci Rep* **7**, (2017).
Maciel, R. *et al.* The human motor neuron axonal transcriptome is enriched for transcripts related to mitochondrial function and microtubule-based axonal transport. *Exp Neurol* **307**, 155 (2018).
Bigler, R. L., Kamande, J. W., Dumitru, R., Niedringhaus, M. & Taylor, A. M. Messenger RNAs localized to distal projections of human stem cell derived neurons. *Scientific Reports 2017 7:1* **7**, 1–11 (2017).
Nijssen, J., Aguila, J., Hoogstraaten, R., Kee, N. & Hedlund, E. Axon-Seq Decodes the Motor Axon Transcriptome and Its Modulation in Response to ALS. *Stem Cell Reports* **11**, 1565 (2018).
Farias, J., Holt, C. E., Sotelo, J. R. & Sotelo-Silveira, J. R. Axon microdissection and transcriptome profiling reveals the in vivo RNA content of fully differentiated myelinated motor axons. *RNA* **26**, 595–612 (2020).
Gumy, L. F. *et al.* Transcriptome analysis of embryonic and adult sensory axons reveals changes in mRNA repertoire localization. *RNA* **17**, 85–98 (2011).
Taylor, A. M. *et al.* Axonal mRNA in Uninjured and Regenerating Cortical Mammalian Axons. *The Journal of Neuroscience* **29**, 4697 (2009).

Acknowledgments: This research was partially supported by HPC OCÉANO (FONDEQUIP Nº EQM170214) and the supercomputing infrastructure of the NLHPC (CCSS210001)

Funding:
ANID projects Fondecyt Initiation 11220601 (A.L.); EMBO scientific exchange grant 9218; EMBO short-stay Fellowship 8263

Author contributions.
Examples: AL, JPR
Conceptualization: AL, AC, RHM.
Methodology: AL, TA, APL, CG, CC, FB, JG, WA, AW, ACH, DC.
Investigation: AL, WZ, RHM, UH, CGR, ACH, AF, JPR.
Visualization: AL, CGR, AC.
Supervision: AL, AC, UH, WZ, CG, APL.
Writing—original draft: AL, AC.
Writing—review & editing: AL, AC, CG, RHM, UW, CGR.

Competing interests: Authors declare that they have no competing interests.

Data and materials availability: All data needed to evaluate the conclusions in the paper will be available upon request.

964
965 **Tables and Figures**
966
967

Study	Neuron cell type	Model to obtain axonal fraction
Saal 2014[84]	Mice motor neurons	Spinal cord motor neurons cultured in microfluidic chambers (7 DIV).
Rotem 2017[85]	Mice motor neurons	Spinal cord motor neurons cultured in porous membrane inserts (10 DIV).
Maciel 2018[86]	iPSC-derived human motor neurons	Motor neurons were cultured on porous membrane inserts (10 DIV)
Bigler 2017[87]	Glutamatergic neurons differentiated from human embryonic stem cells (hESCs)	hESCs differentiated for 59 DIV in microfluidic chambers.
Nijssen 2018[88]	Human and mice motor neurons.	Spinal cord and human stem cell derived motor neurons were cultured in microfluidic chambers (7 and 14 DIV, respectively).
Farías 2020[89]	Rat mature myelinated motor neurons	Axoplasm microdissection of motor axons (*Ex-vivo)*.
Gumy 2010[90]	Rat embryonic/adult sensory neurons from dorsal root ganglion (DRG)	Primary neurons were cultured in microfluidic chambers (4 DIV).
Taylor 2009[91]	Uninjured and regenerating rat cortical neurons	Primary neurons cultured in microfluidic chambers (10 DIV).

968 **Table I.** Analyzed publications examining the transcriptome of an axon-enriched neuronal
969 fraction. Days *in vitro* (DIV).
970
971

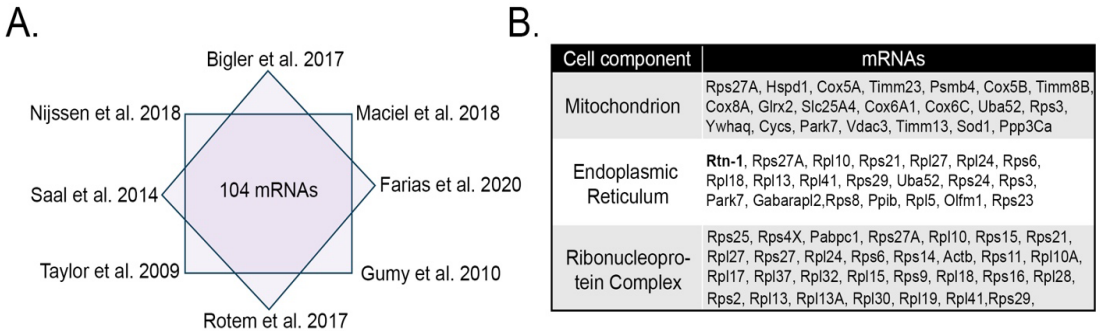

972
973 **Figure 1.** Analysis of axonal transcriptomes reveals that ER mRNAs are a relevant category and
974 Rtn-1 mRNA is consistently present across samples. **A.** Scheme summarizing key studies on
975 axonal transcriptomes and the shared mRNAs identified. **B.** Table listing the category "Cellular
976 Component" (Gene Ontology, GO) terms to classify the 104 common mRNAs found in axonal
977 transcriptomes. The endoplasmic reticulum (ER) category reveals that the mRNA coding for Rtn-
978 1 (bold) is the only common ER structural protein identified.

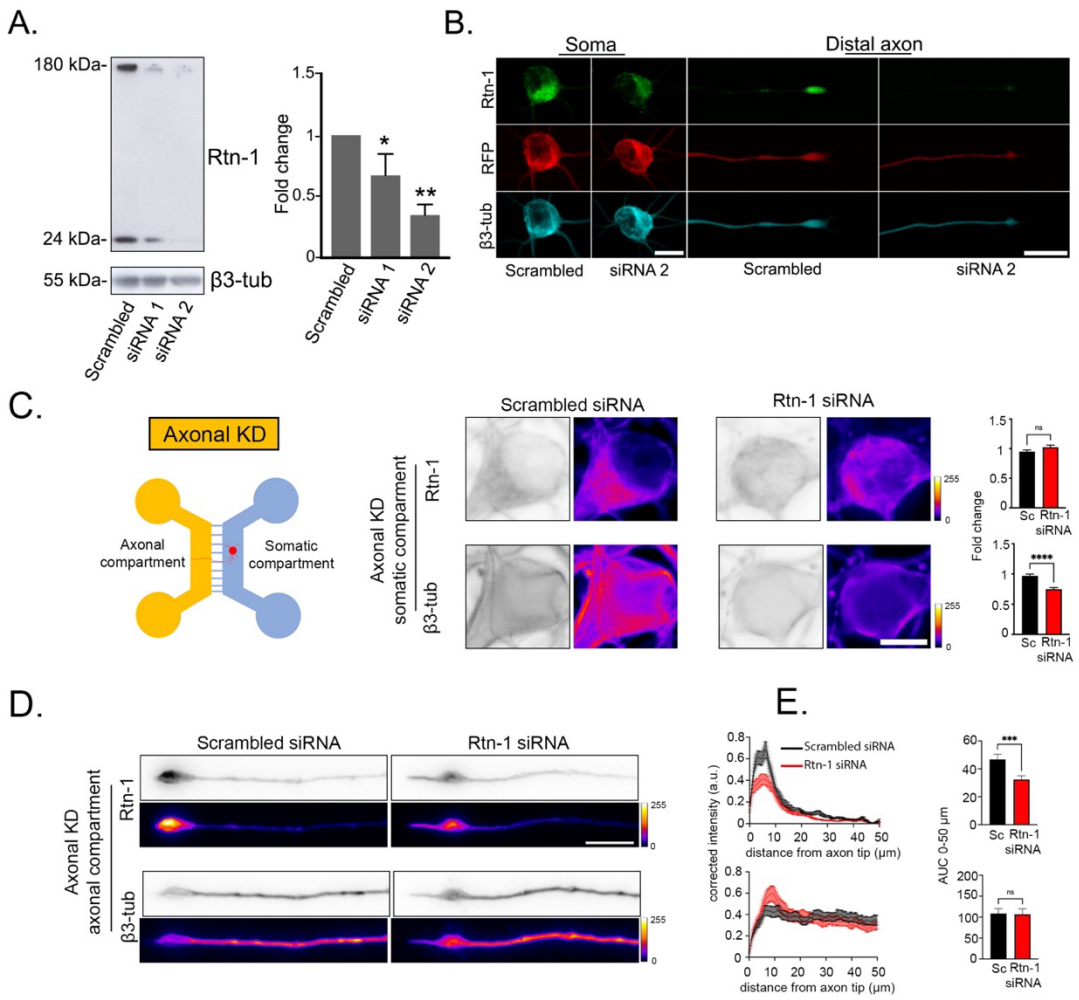

Figure 2. Axonal synthesis of Rtn-1 can be independently regulated in cortical neurons. **A.** Western blot analysis confirming the knockdown efficiency of Rtn1-siRNA in 7-9 DIV cortical neurons, with β3-tubulin as the loading control. The graph on the right quantifies lower molecular weight Rtn1 expression relative to β3-tubulin. Data are displayed as mean ± standard error of N = 6 biological replicates. Wilcoxon test compared to a theoretical mean of 1; $*p < 0.05$; $**p < 0.01$. **B.** Immunofluorescence images of the soma and distal axon of neurons treated with a plasmid encoding RFP and control (scrambled, Scr) or Rtn-1-siRNA, demonstrating the effect of Rtn1 knockdown along with β3-tubulin and RFP expression. Representative images from N= 4 independent experiments**.** Bar=20 μm **C.** Schematic representation of the axonal knockdown strategy in microfluidic chambers alongside fluorescence images and quantitative analysis of Rtn1 and β3-tubulin intensity in the somatic compartment. Bar=10 μm. Data are displayed as mean ± standard error of 229-300 neurons from N = 3 biological replicates. Mann-Whitney test; $****p < 0.0001$. **D.** Immunofluorescence showing the relative levels of Rtn1 and β3-tubulin along the last 50 μm of axons from cortical neurons locally transfected with Scr or Rtn1-siRNA. Bar=10 μm **E.** Intensity profiles and quantitative analysis showing the relative levels of axonal Rtn1 and β3-tubulin following knockdown compared to control. Data are displayed as mean ± standard error of 87-102 axons from N = 3 biological replicates. Mann-Whitney test; n.s., not

significant;∗∗∗p < 0.001.

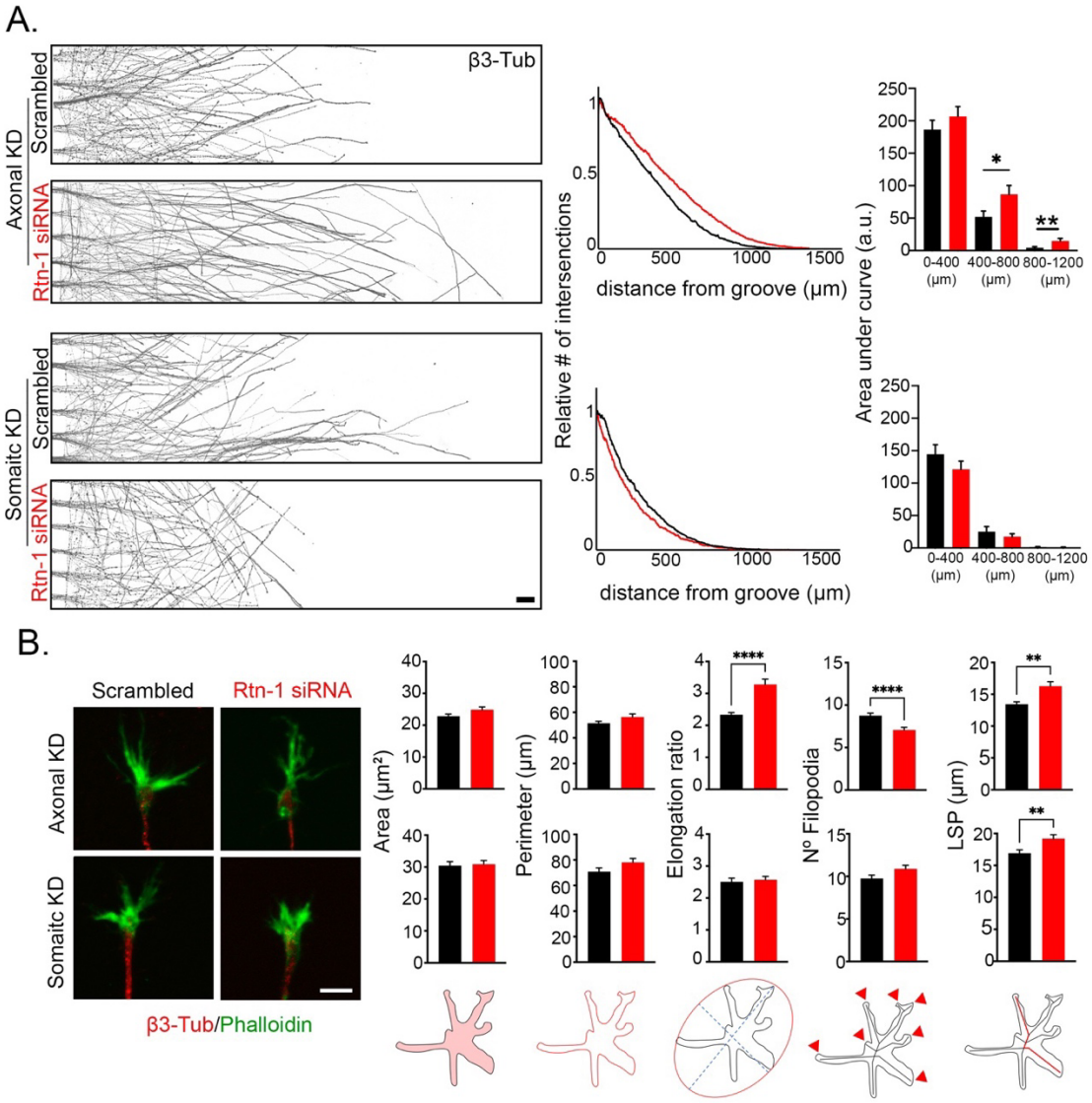

Figure 3. Axonal Rtn-1 KD promotes outgrowth and modify GC cytoskeleton after injury. **A.** Immunofluorescence of β3-Tubulin in axons growing in microfluidic chambers 24 hours after injury (axotomy) comparing axonal and somatic Rtn1 knockdown (Rtn1-siRNA) with control (scrambled, Scr). Bar= 50 µm. The accompanying graphs show the relative number of axonal intersections and counts at increasing distances from the soma as the area under curve (AUC) of indicated segments. Data are displayed as mean ± standard error of 23-24 axonal fields from N = 6 biological replicates for axonal KD; and 18-20 axonal fields from N=3 biological replicates for somatic KD. Mann-Whitney test; ∗p < 0.05; ∗∗p < 0.01.**B.** Morphological analysis of growth cones in axon and somatic regions labeled with β3-Tubulin and phalloidin. Bar= 5 µm. Graphs depict differences in growth cone area, perimeter, and complexity metrics such as elongation ratio (aspect ratio), number of filopodia, and longest shortest path (LSP, skeleton), from axons treated with Rtn1-siRNA and Scr. The schematic drawings illustrate the morphological features observed under each condition. Data are displayed as mean ± standard error of 145-153 axons for axonal

KD; 227-148 axons for somatic KD from N = 3 biological replicates. Mann-Whitney test; ∗∗p < 0.01; ∗∗∗∗p < 0.0001.

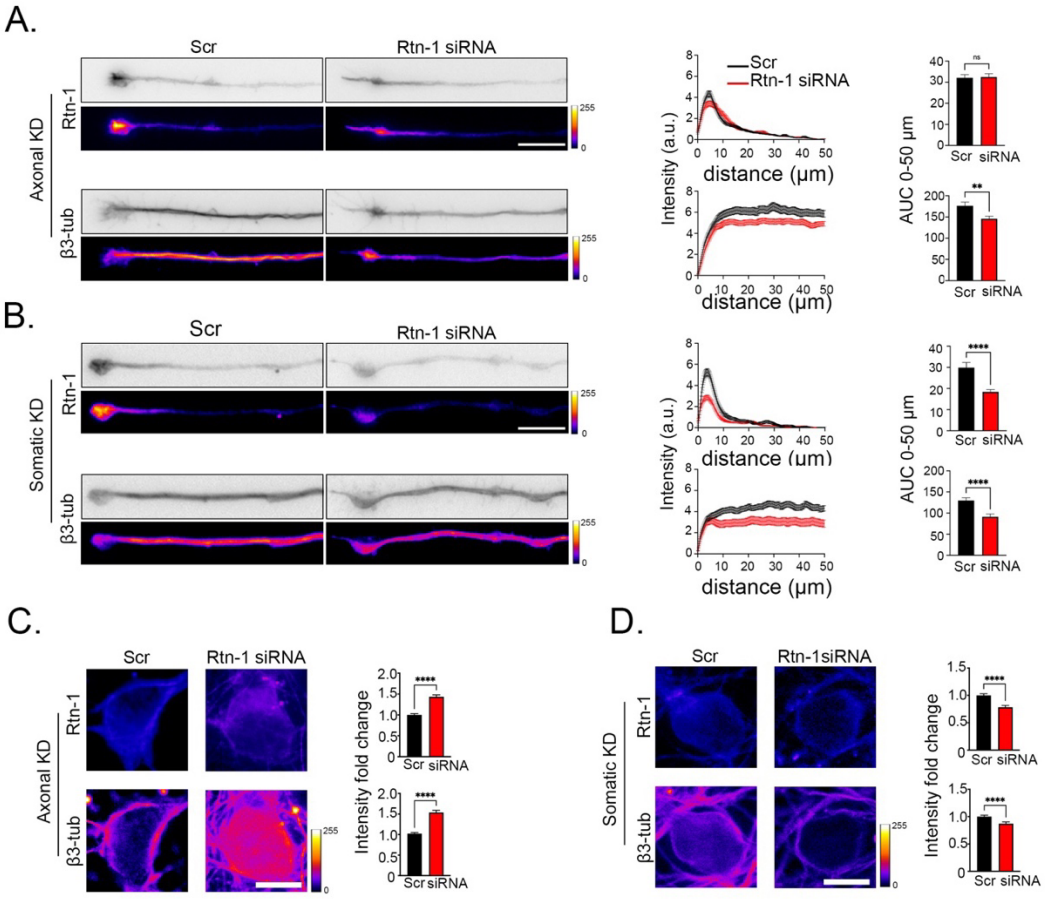

Figure 4. Microtubule levels of injured axons depend on local Rtn-1 synthesis. **A.** Immunofluorescence and intensity profiles of axons stained for Rtn1 and β3-Tubulin after axonal transfection with Rtn1 siRNA (axonal Rtn-1 KD) versus a control siRNA sequence (Scr). Fluorescence intensity profile across axonal length and the graphs quantifying the area under the curve (AUC) are indicated. Bar=10 μm. Data are displayed as mean ± standard error oof 206-242 axons from N = 3 biological replicates. Mann-Whitney test; ∗∗p < 0.01. **B.** Analysis of axons stained for Rtn-1 and β3-Tubulin after somatic transfection with Rtn1 siRNA (somatic Rtn-1 KD) versus scr. Fluorescence intensity profile across axonal length and the graphs quantifying AUC are indicated. Bar=10 μm. Data are displayed as mean ± standard error of 133-161 axons from N = 3 biological replicates. Mann-Whitney test; ∗∗∗∗p < 0.0001 **C.** Images depict neuronal cell bodies stained for Rtn-1 and β3-Tubulin, bar graphs indicate the fold change quantification of Rtn-1 and β3-Tubulin after axonal Rtn-1 KD versus scr. Bar=10 μm. Data are displayed as mean ± standard error of 358-382 neurons from N = 3 biological replicates. Mann-Whitney test; ∗∗∗∗p < 0.0001 **D.** Neuronal cell bodies stained for Rtn-1 and β3-Tubulin are indicated, bar graphs indicate the fold change quantification of Rtn-1 and β3-Tubulin after somatic Rtn-1 KD versus

scr. Bar=10 µm. Data are displayed as mean ± standard error of 252-237 neurons from N = 3 biological replicates. Mann-Whitney test; ****p < 0.0001.

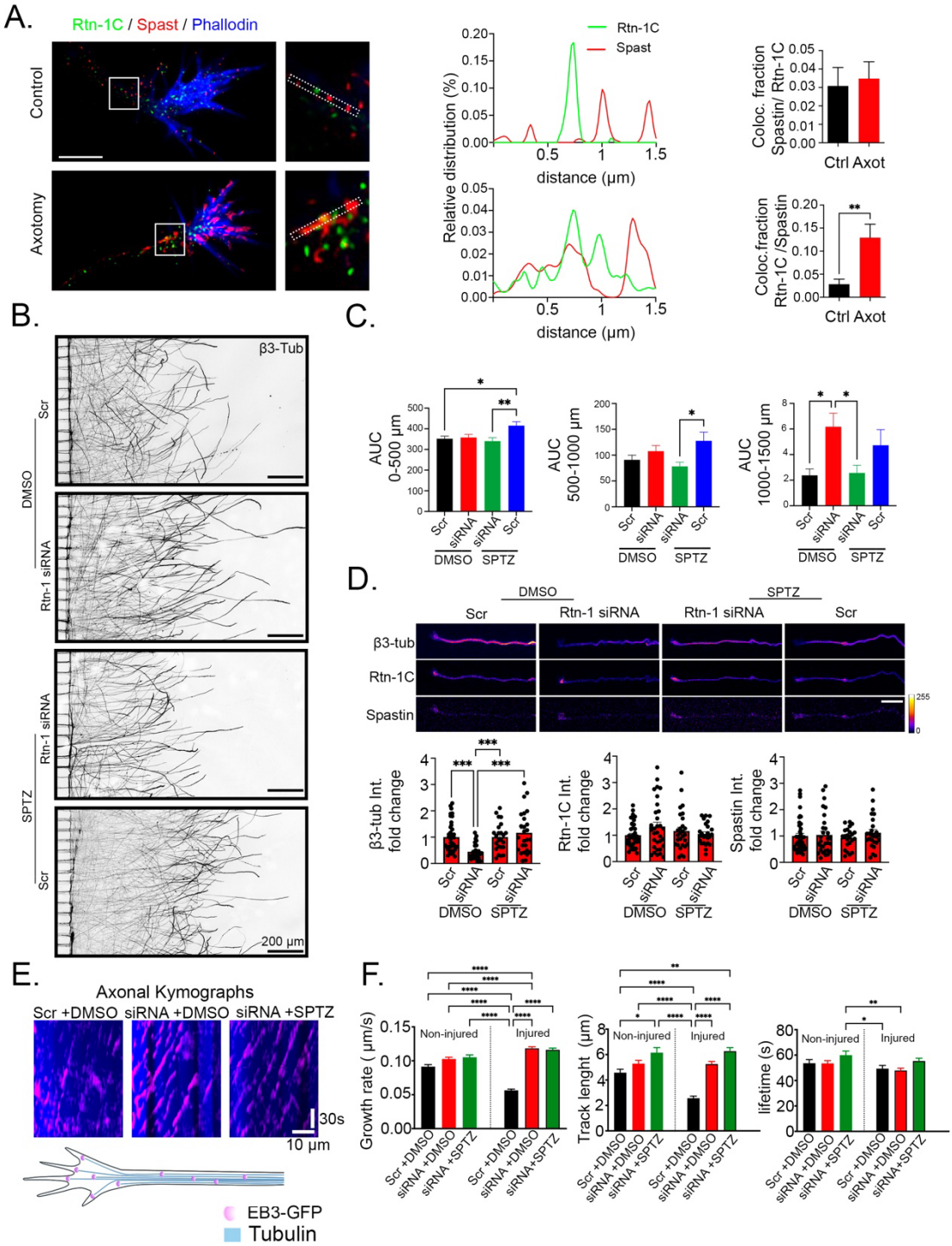

Figure 5. Axonal Rtn-1 KD increases outgrowth by promoting Spastin's microtubule severing. **A.** Representative fluorescent STED images of distal axons from microfluidic chambers containing control cortical axons or forty-four hours post-axotomy, which were stained for Rtn-1C (green), Spastin (red), and F-actin (phalloidin, blue). Insets show colocalization of Rtn-1C and Spastin. Right: Line scan analysis of Rtn-1C and Spastin highlighted in the white rectangle and

their distribution along the axon. Bar graphs show the quantification of colocalization in control and axotomy conditions. Scale bar= 5 µm. Data are displayed as mean ± standard error of 6-7 axons. Unpaired t test; $**p < 0.01$ **B.** Representative images of axonal fields from microfluidic chambers 48 hours post-axotomy under different treatments: control sequence (Scrambled, Scr), Rtn-1 knockdown (Rtn-1 siRNA), and Spastin pharmacological inhibition (SPZT), and labeled with β3-tubulin (β3-tub). Scale bar represents 200 µm. **C.** Quantification of axon outgrowth under the treatments shown in A. The Area under the curve (AUC) was measured as the sum of the relative number of intersections at different distance ranges from the groove in the microfluidic chambers (0-500 µm; 500-1000 µm and 1000-1500 µm). Scale bar represents 10 µm. Data are displayed as mean ± standard error of 22-24 axonal fields for condition from N=3 biological replicates. One-way ANOVA followed by Tukey's posthoc test; $*p < 0.05$; $**p < 0.01$. **D.** Fluorescence intensity profiles of β3-tubulin, Rtn-1C, and Spastin in axons and quantifications of intensity changes of indicated proteins as the fluorescence AUC fold change of the last 50 µm compared to Scr. Data are displayed as mean ± standard error of 24-40 axons for condition from N=3 biological replicates. Kruskal-Wallis followed by Dunn's posthoc test; $***p < 0.001$ **E.** Axonal kymographs showing dynamic microtubule behavior in neurons with indicated treatments after axotomy, dashes represent the traces of EB3-GFP (end-binding protein 3). Scale bars represent 10 µm and 30 seconds, respectively. **F.** Analysis of microtubule dynamics parameters in non-injured and injured axons with different treatments: growth rate, track length, and lifetime of microtubule plus-end tracks. Data are displayed as mean ± standard error of 146-377 comets for condition from N=3 biological replicates. Kruskal-Wallis followed by Dunn's posthoc test; $*p < 0.05$; $**p < 0.01$; $****p < 0.001$.

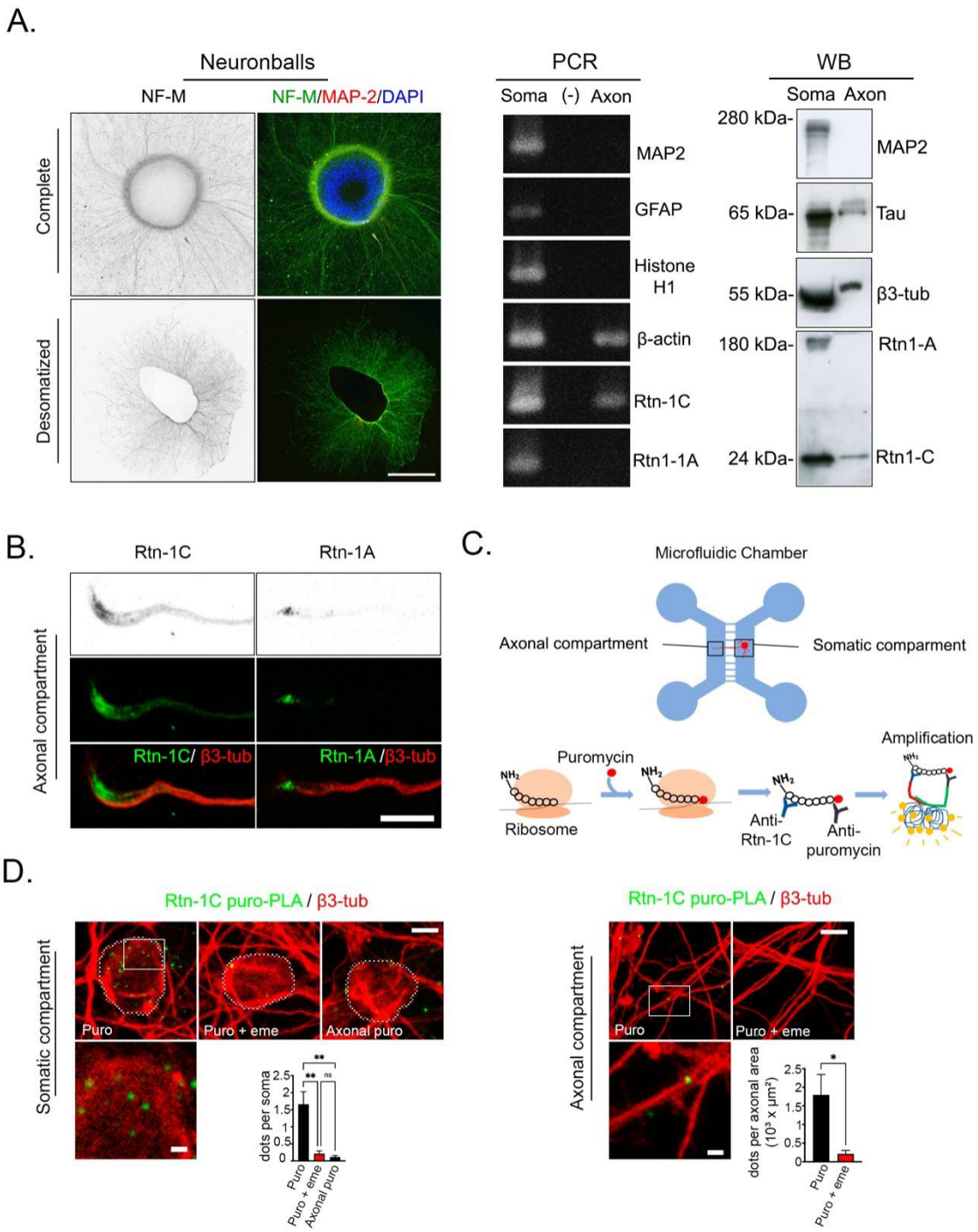

Figure 6. Rtn-1C is locally synthesized in cortical axons. **A.** Neuronball formation and subcellular fractionation. Left: Immunocytochemistry of neuronballs stained with neurofilament medium chain (NF-M, grayscale) and double-stained with NF-M/Microtubule-associated protein 2 (MAP-2, green) with nuclei counterstaining (DAPI, blue). Top panel shows intact neuronballs, bottom panel shows neuronballs after mechanic removal of cell bodies. Right: Corresponding RT- PCR and Western Blot (WB) analyses of axonal and somatic fractions for MAP2, glial fibrillary acidic protein (GFAP), histone H1, β-actin, Rtn-1C, and Rtn-1A. Scale bar represents 500 µm. Images and blots are representative of two independent experiments. **B.** Confocal images showing the expression of Rtn-1C and Rtn-1A (green) in axonal compartment of microfluidic chambers, with

β3-tubulin (β3-tub, red) as a neuronal marker. Scale bar represents 10 µm. Images are representative of two independent experiments **C.** Schematic of the microfluidic chamber setup used to separate axonal and somatic compartments, with the mechanism of puromycin labeling depicted to the right. Puromycin (Puro) incorporation into newly synthesized proteins allows for visualization of translation and proximity ligation assay (PLA) allows for Rtn-1C recognition. **D.** PLA positive spots are shown in green at somatic and axonal compartments. β3-tubulin labeling depicts cell bodies and axons. Insets show higher magnification of PLA signals. Quantification of dot signals per area in somatic and axonal compartments with and without emetine (eme) treatment, indicating active translation sites. Scale bars= 5 µm; inserts= 1 µm. Data are displayed as mean ± standard error of four independent experiments. One-way ANOVA followed by Tukey's posthoc test; $**p < 0.01$. Unpaired t test; $*p < 0.05$.

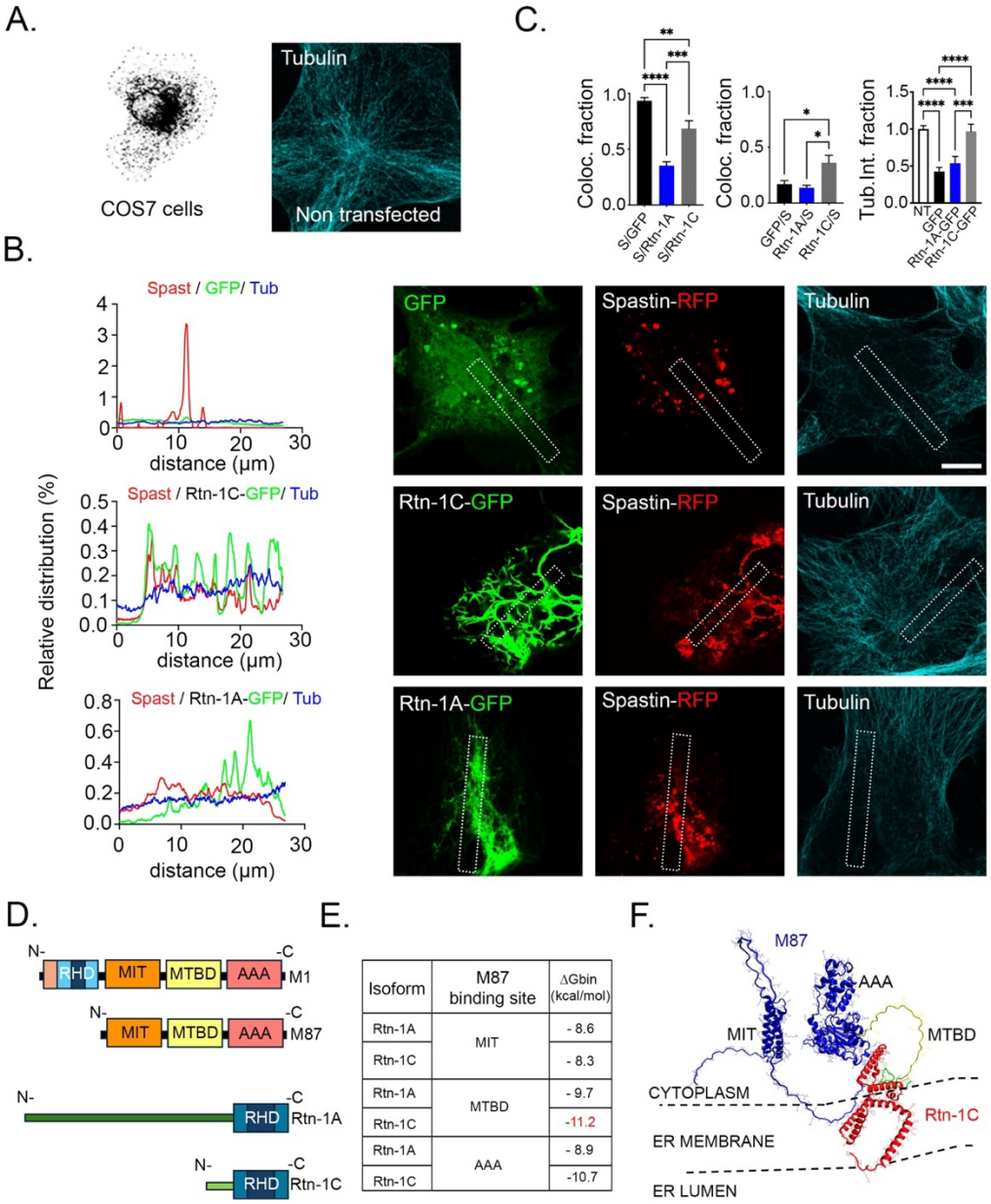

Isoform	M87 binding site	ΔGbin (kcal/mol)
Rtn-1A	MIT	- 8.6
Rtn-1C		- 8.3
Rtn-1A	MTBD	- 9.7
Rtn-1C		-11.2
Rtn-1A	AAA	- 8.9
Rtn-1C		-10.7

1086 Figure 7. Rtn-1C co-distributes with Spastin decreasing microtubule severing activity. **A.**
1087 Fluorescent staining of tubulin depicting microtubules in non-transfected COS7 cells. **B.**
1088 Fluorescence imaging and relative distribution analysis of Spastin-RFP and co-expression with
1089 Rtn-1C-GFP or Rtn-1A-GFP in relation to tubulin. Line scans show the distribution of
1090 fluorescence intensity across the area enclosed by the white rectangles. **C.** Left panel shows the
1091 colocalization quantification of GFP, Spastin-RFP with Tubulin, and Reticulon isoforms
1092 expressed as colocalized fraction. Right panel indicates the changes in tubulin intensity associated
1093 with Spastin expression in comparison with non-transfected cells (shown in A). For colocalization
1094 analysis, data are displayed as mean ± standard error of 9 Spastin-RFP/GFP cells; 9 Spastin-RFP/
1095 Rtn-1A-GFP cells, and 9 Spastin-RFP/ Rtn-1C-GFP cells from two independent experiments.
1096 One-way ANOVA followed by Tukey's posthoc test; $**p < 0.01$; $*** p < 0.001$; $**** p < 0.0001$.
1097 For tubulin intensity analysis, data are displayed as mean ± standard error of 145 non-transfected
1098 cells, 33 Spastin-RFP/GFP cells, 35 Spastin-RFP/ Rtn-1A-GFP cells, 32 Spastin-RFP/ Rtn-1C-
1099 GFP cells from two independent experiments. One-way ANOVA followed by Tukey's posthoc
1100 test; $*p < 0.05$; $**p < 0.01$; $*** p < 0.001$; $**** p < 0.0001$. **D.** Schematic representation of
1101 Spastin, Rtn-1A and Rtn-1C protein domains including RHD (Reticulon Homology Domain),
1102 MIT (Microtubule Interacting and Trafficking molecule), MTBD (Microtubule Binding Domain),
1103 and AAA (ATPases Associated with diverse cellular Activities). **E.** Table listing the binding site
1104 affinities (in kcal/mol) for the M87 binding site on Reticulon isoforms, indicating their potential
1105 interaction strength. **F.** VMD snapshots of a structural model illustrating the interaction between
1106 the N-terminal domain of Rtn-1C (light green) and the M87 MTBD (yellow).